*minerals*

MDPI

*Article*

# Petrological Studies and Geochemical Modelling of Water–Rock Interactions in the Grønnedal-Íka Alkaline Complex Generating Ikaite Deposition in Ikka Fjord, SW Greenland

**Sigríður María Aðalsteinsdóttir [1,*], Gabrielle J. Stockmann [1], Erik Sturkell [2], Enikő Bali [1], Guðmundur H. Guðfinnsson [1] and Andri Stefánsson [1]**

[1] Institute of Earth Sciences, University of Iceland, Sturlugata 7, 102 Reykjavík, Iceland; gabrielle@hi.is (G.J.S.); eniko@hi.is (E.B.)
[2] Department of Earth Sciences, University of Gothenburg, 413 20 Gothenburg, Sweden
* Correspondence: sigridurma@hi.is

**Abstract:** The Mesoproterozoic alkaline Grønnedal-Íka complex (1325 ± 6 Ma) is intruded into old Archean gneissic bedrock between Ikka Fjord and Kangilinnguit (Grønnedal) by Arsuk Fjord in Southwestern Greenland. This 8 × 2.8 km oval-shaped complex constitutes the oldest part of the Gardar Province, representing a failed continental rift across southern Greenland. It comprises outer rings of mainly nepheline syenites with a central plug of Fe- and Ca-rich carbonatites. Here, we present petrological data on the syenites and carbonatites combined with geochemical modelling of groundwater percolating through the Grønnedal-Íka complex and the secondary minerals and fluid chemistry arising from these fluid–rock reactions. The results show that modelling using input data of (1) meteoric water in a closed system with respect to atmospheric $CO_2$ can (2) dissolve the primary minerals of the syenites and carbonatites and (3) simulate the fluid chemistry of the natural sodium carbonate springs of 3–4 °C and pH 10–11 seeping up through fractures at the bottom of Ikka Fjord, which (4) leads to the deposition of nearly a thousand tufa columns of the cold carbonate mineral ikaite ($CaCO_3 \bullet 6H_2O$). Our results thereby support the geochemical relationship between fluid–rock reactions inside the Grønnedal-Íka alkaline complex and the precipitation of ikaite in the shape of submarine tufa columns in Ikka Fjord. The modelling indicates that the groundwater itself can be supersaturated with respect to ikaite and provide the seed crystals that lead to the columnar growth of ikaite up to 20 m tall in the seawater of Ikka Fjord.

**Keywords:** Grønnedal-Íka alkaline complex; nepheline syenite; carbonatite; alkaline groundwater; ikaite; Ikka Fjord; fluid–rock interaction

check for updates

Academic Editor: Huifang Xu

Received: 27 February 2025
Revised: 28 March 2025
Accepted: 29 March 2025
Published: 2 April 2025

**Citation:** Aðalsteinsdóttir, S.M.; Stockmann, G.J.; Sturkell, E.; Bali, E.; Guðfinnsson, G.H.; Stefánsson, A. Petrological Studies and Geochemical Modelling of Water–Rock Interactions in the Grønnedal-Íka Alkaline Complex Generating Ikaite Deposition in Ikka Fjord, SW Greenland. *Minerals* **2025**, *15*, 373. https://doi.org/10.3390/min15040373

**Copyright:** © 2025 by the authors. Licensee MDPI, Basel, Switzerland. This article is an open access article distributed under the terms and conditions of the Creative Commons Attribution (CC BY) license (https://creativecommons.org/licenses/by/4.0/).

## 1. Introduction

The motivation for this study is the presence of close to a thousand tufa columns rising from the bottom of the shallow Ikka Fjord in southwest Greenland. These columns, some up to 20 m tall and 8 m wide, are composed primarily of the metastable mineral ikaite ($CaCO_3 \bullet 6H_2O$) [1–5]. While the presence of these structures is well documented, the geochemical processes and fluid–rock interactions driving their formation remain insufficiently understood. This study aims to address this gap through geochemical modelling. The formation of ikaite in this fjord is favoured by low seawater temperatures (0–6 °C) and sodium carbonate–bicarbonate-rich groundwaters with an alkaline pH of 10–11 and constant temperatures of 3–4 °C. When the groundwater mixes with

the seawater of the fjord, it creates supersaturation with respect to ikaite, leading to the precipitation of the columns [1–3]. The precipitation of ikaite can be simplified by the reaction $Ca^{2+} + 2HCO_3^- + 4H_2O \rightarrow CaCO_3 \cdot 6H_2O$ (ikaite) + $CO_2$, where calcium ions and bicarbonate from the alkaline groundwater combine under low temperatures to form ikaite.

Chemical and isotope data suggest that the alkaline groundwaters are formed as the result of water–rock interactions inside the Grønnedal-Íka alkaline complex through reactions of the nepheline syenites and calcium- and iron-rich carbonatites with meteoric water percolating through fractures in the complex [1,2]. The study by Tollefsen et al. (2019) [6] showed that secondary alteration of the nepheline syenites leads to the release of sodium ($Na^+$) into the groundwater by the replacement of nepheline by illite and analcime. Simultaneous alteration of the Fe-rich parts of the carbonatites leads to the release of bicarbonate ions into the groundwater by oxidation of siderite to goethite, creating alkaline groundwater [6].

While previous studies have been focused on the physical and chemical conditions of ikaite formation, there remains a knowledge gap regarding the detailed geochemical pathways that generate these alkaline groundwaters—particularly in the context of fluid–rock interaction modelling. Understanding this connection is essential to explain the formation of ikaite columns and assess their stability under changing environmental conditions. The objective is therefore to model the secondary fluids and mineral formation in the Grønnedal-Íka complex resulting from meteoric water interactions with primary minerals using bulk chemical analysis of representative rock samples of the complex. In this study, the focus was on using as unaltered nepheline syenite and carbonatite samples as possible. Major and trace element geochemistry of the selected rock samples were defined through a combination of petrographical, mineralogical, and bulk chemical analysis. Geochemical reaction path modelling of the major element chemistry of the rock samples was undertaken to calculate the simulated major elemental signatures of the secondary fluids. Presented here are the first-ever attempts at simulating the mineral–fluid reactions leading to the creation of sodium carbonate groundwaters. The modelling is subsequently appraised as to whether these processes lead to the saturation of ikaite when mixed with seawater.

### *1.1. The Grønnedal-Íka Complex and the Gardar Province*

The Grønnedal-Íka alkaline complex of syenites and carbonatites is one of more than 10 intrusions formed during the breakup of the supercontinent Columbia, producing a rift system that extended across eastern Canada, southern Greenland, and beyond to Finland, measuring a distance of some 5000 km today [7–9]. Alkaline intrusions, such as the Grønnedal-Íka complex, are key features of rift-related magmatism and provide important insights into mantle enrichment and continental extension processes in action. These complexes are often enriched in rare earth and high-field-strength elements and can exhibit unique mineralogy and alteration histories. The role of alkaline magmatism in continental rift settings has been highlighted in global contexts, such as the Indian Shield [10,11], as offering comparative insights into the geodynamic setting and magmatic evolution of rift-related complexes like those of the Gardar Province.

Zircons extracted from the Grønnedal-Íka syenites have provided the U-Pb age of 1325 ± 6 Ma [12], which makes it the oldest detected magmatic activity at the onset of the Gardar continental rift. Other Gardar intrusions in the vicinity of the Grønnedal-Íka complex are the Ivigtût cryolite ($Na_3AlF_6$) body (1264 ± 8 Ma, ([13] and references therein)), 7 km distant, and the Kûngnât syenite complex (1275 ± 1.8 Ma on gabbro ring dykes [14]), at 19 km distant (see Figure 1). Other well-known Gardar intrusions include the Ilímaussaq complex near the town of Narsaq (Figure 1). Nearly all the Gardar intrusions are characterized by unusual mineralogy, high contents of rare earth elements (REEs), and high-field-strength elements (HFSEs), currently in high demand due to their important roles in

the green technology and energy transition industries [13]. Several REE-rich minerals have been identified in the carbonatites of the Grønnedal-Íka complex as fine-grained minerals of, e.g., REE fluorocarbonates (parisite, synchysite, röntgenide) and monazites, which occur together with strontianite, barite, and apatite [15]. Apatite is one likely primary REE source, which was mobilized by late-stage hydrothermal fluids, with the REE precipitated as separate secondary minerals, i.e., the REE minerals listed above [15]. It should be noted here that the spellings used throughout this text for the names of geological intrusions, e.g., Ivigtût, are the names used in these often quite dated publications, whereas, when referencing geographical places, the new spellings of these locations are used, e.g., the town of Ivittuut.

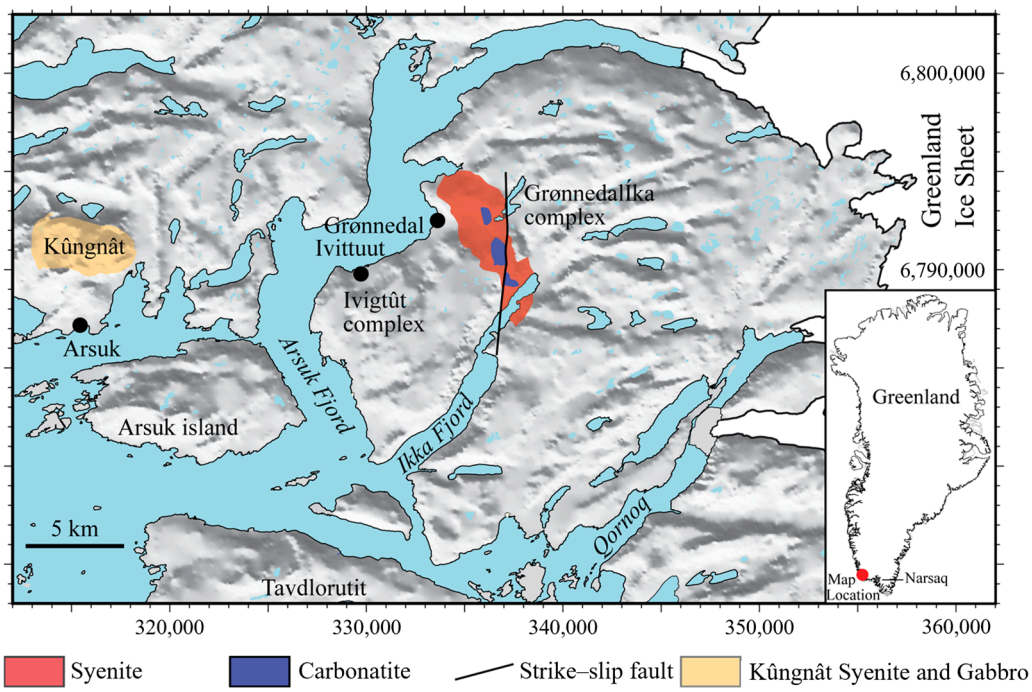



**Figure 1.** Location of Ikka Fjord, Arsuk Fjord, and the towns of Grønnedal, Ivittuut, and Arsuk in SW Greenland. The red- and blue-coloured areas mark the Grønnedal-Íka complex, the yellow area marks the Kûngnât complex, and the grey areas consist of old Archean gneissic rocks and Ketilidian meta-volcanics. The Ivigtût complex is within the borders of the black circle marking the mining town of Ivittuut.

Southern Greenland comprises three major geological units: the Archean craton (3200–2600 Ma), the Palaeoproterozoic Ketilidian of meta-sediments and meta-volcanic rocks (c. 1800 Ma) [16,17]), and the Mesoproterozoic Gardar Province (1325–1140 Ma) [18,19]. The southernmost part of the Ketilidian encompasses the Julianehåb batholith of granite and folded psammites and pelites at the southern tip of Greenland. The latter two were intruded by near-contemporaneous granites [20]. The Ikka and Arsuk Fjord areas are situated on the boundary zone where the Gardar continental rifting started to break apart the old suture of the Archean craton and the subducted Ketilidian border zone. In this area, the three Gardar complexes intruded into a basement of Archean gneisses with patches of Ketilidian crystalline meta-volcanic rocks, e.g., on Arsuk Island [16,21].

Between the naval base at Grønnedal (Kangilinnguit) in Arsuk Fjord and the shores of Ikka Fjord (Figure 1), the ground rises to an 800 m plateau of Archean gneisses encompassing the 500 m high Grønnedal-Íka complex that is crisscrossed by several dykes of Gardar age (Figure 2).

Three generations of dolerite dykes intruded the complex as part of the Gardar rifting activities at 1284–1268 Ma [22]. These include a 55 m wide olivine dolerite dyke that cuts

through the central carbonatite body and then acts as a conduit for fluids enriched in fluorine (F) and $CO_2$ [23]. Substantial amounts of magnetite have formed through the oxidation of siderite at distances of up to 40 m from the contacts between the dolerite dike and the carbonatite [21,23]. The dikes formed before the complex was tectonically deformed. Emeleus and Upton (1976) [19] reconstructed the faulting history of the Grønnedal-Íka complex into three major steps with mainly strike–slip displacements. Furthermore, Emeleus (1964) [21] described several 0.5–15 m wide lamprophyre, trachyte, and phonolite dykes cutting the complex. These dykes are also related to Gardar rifting.

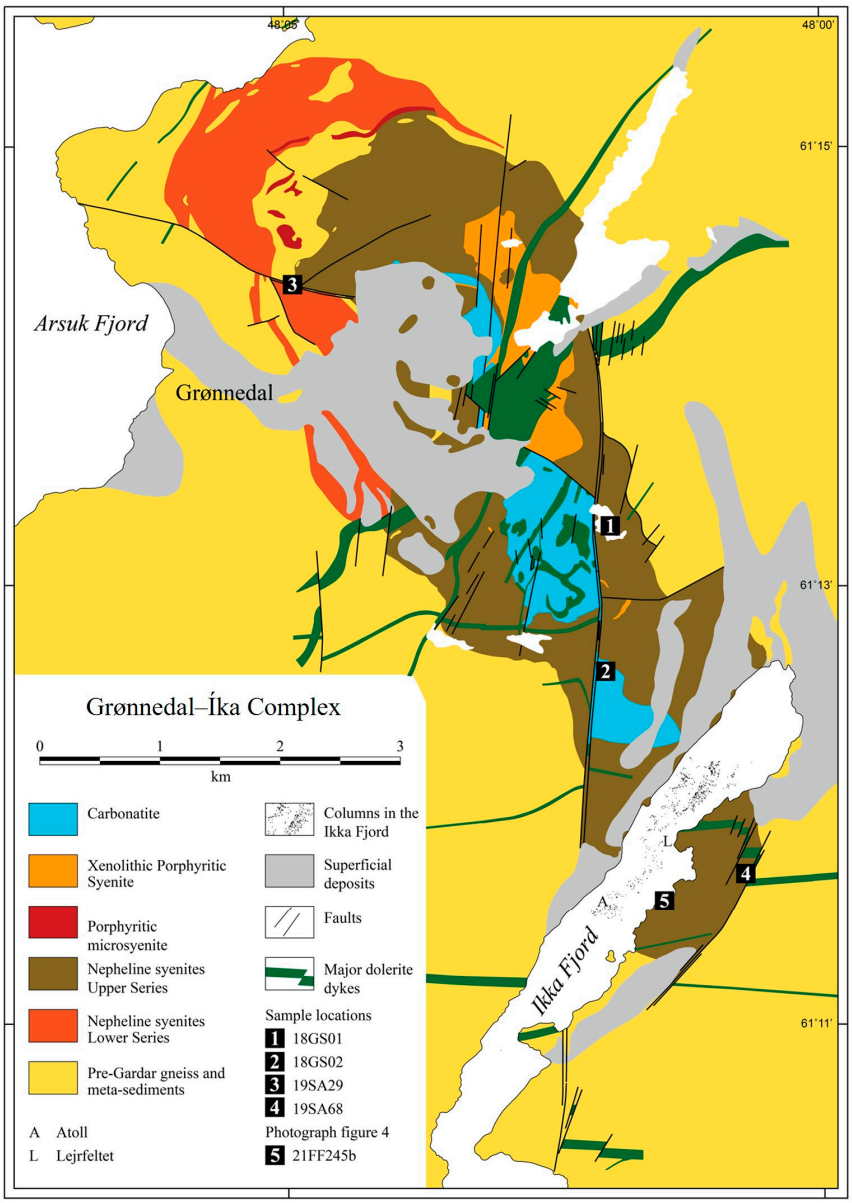



**Figure 2.** Simplified geological map of the Grønnedal-Íka complex, modified after Emeleus (1964) [21]. Locations of rock samples collected for this study are labelled by numbers 1–5. The map faces north and is referenced in UTM-WGS84.

The Grønnedal-Íka complex of today has an elliptic shape of 8 × 2.8 km, which has been elongated from an original ovoid intrusion of 5.9 × 3.5 km through tectonically induced displacement and faulting. Carbonatites make up the core of the intrusion, surrounded by several rings of syenites of different chemical compositions (Figure 2) [21]. Emeleus (1964) [21] suggested the following sequence for the formation of the Grønnedal-

Íka igneous complex: An initial suite of layered nepheline syenites was intruded by late xenolithic porphyritic syenite and, finally, a central body of carbonatite was formed by explosively intruding into the still hot rock suites of syenites. The syenite rocks are divided into Lower and Upper Series (Figure 2), with the Lower Series being the oldest. The majority of the syenites in the Grønnedal-Íka complex are foid syenites [21]. Xenolithic syenites intruded into the layered Lower and Upper Series at a later stage [21]. A study based on REE by Bedford (1990) [24] suggested that the nepheline syenites were derived from a parental magma formed by a few per cent partial melting of a garnet lherzolite mantle source during the early Gardar rifting. A new study based on Nd-Hf isotopes [13] found that the Gardar Province melt source became enriched in REE and HFSE during the Paleoproterozoic when subduction-derived fluids mobilized metals from a mantle wedge in the asthenosphere. The metals were trapped via metasomatism of the lithospheric mantle, forming phlogopite–ilmenite–clinopyroxene-bearing veins. During the Mesoproterozoic continental rifting, this metasomatized lithospheric mantle melted and formed the Gardar Province with its large REE and HFSE deposits [13].

The nepheline syenites in the Grønnedal-Íka complex are mainly composed of four primary minerals: nepheline, alkali feldspar, clinopyroxene, and biotite. The nepheline ($(Na,K)AlSiO_4$) is a feldspathoid mineral, the alkali feldspar mineral is orthoclase ($KAlSi_3O_8$) with perthite structure, and the clinopyroxene mineral is aegirine–augite ($(NaCaFe^{2+}Mg)(Fe^{3+}AlFe^{2+}Mg)Si_2O_6$). In addition, biotite ($K(Mg,Fe)_3AlSi_3O_{10}(F,OH)_2$) is common in these rocks [8]. The carbonatites are mainly composed of calcite ($CaCO_3$) and siderite ($FeCO_3$), together with Fe oxides of magnetite ($Fe_3O_4$) and hematite ($Fe_2O_3$) [21]. The high content of Fe-rich carbonatites makes them unusual compared to other carbonatites of the world [23,25].

### *1.2. Ikka Fjord and the Ikaite Columns*

Ikka Fjord is close to 13 km long and oriented in a SW–NE direction (Figure 2). In the innermost 3 km of the fjord, Seaman et al. (2022) [26] mapped 938 columns of 0.5–20 m height with Multibeam Sonar Equipment (MBES) in the summer of 2019. Figure 2 depicts the distribution of columns in the fjord (black dots). The most massive column is found at the continuation of one of the major strike–slip faults that cut the Grønnedal-Íka alkaline complex (Figure 1). The columns only exist in the proximity of the Grønnedal-Íka syenites and carbonatites; no columns are found where the bedrock changes to gneissic (Figure 2). Furthermore, the runoff water passing over the gneissic rocks is almost electrolyte-free, while the water draining the complex is slightly alkaline to alkaline [2]. This supports the theory that there is a close geochemical link between the petrology of the complex and the distribution and existence of the ikaite tufa columns in Ikka Fjord [12]. Isotope studies further strengthen the link. The $^{14}C$ dating of the ikaite detects 'dead' carbon, pointing to the old Proterozoic carbonatite as the C source [2]. A recent study by Buchardt et al. (2024) [27], using stable isotope data ($\delta^{18}O$ and $\delta^{2}H$) of rivers, streams, seawater, and column water, showed a meteoric origin of the alkaline groundwater seeping up through the columns identical to that of the meteoric water collected on top of the 500 m high plateau partly enclosing the Grønnedal-Íka complex. The $\delta^{2}H$ values range from −90.4 to −95.7‰ in the column water and −97.3‰ in the springs, while $\delta^{18}O$ values range from −12.75 to −13.15‰ in the column water and −13.10‰ in the springs [2].

The environmental setting of the fjord is classified as low arctic, with mean temperatures between −1.9 °C and +2.9 °C [28] and no records of current permafrost in the area. The area is generally covered by snow from November to May, and the annual precipitation is ~1000 mm [28]. In the summertime, the seawater is stratified, and the uppermost two meters are almost fresh and originate from the rivers and small springs in the area,

reaching temperatures up to 12 °C. Saltier (up to 33 psu, salt content 33 g per kg of water) and colder (<6 °C) water is found below the halocline [2,5]. This water likely originates from the cold <3 °C East Greenland Current [29]. The sedimentary accumulations on the floor of the fjord are mainly clays with organic debris and drop stones. Where the sedimentary cover is interrupted by the occasional syenite roches moutonneés [3], these break the sedimentary seal and then provide foundations for columns to grow from the artesian flow of spring waters leaking around the rock exposures (Figure 3).

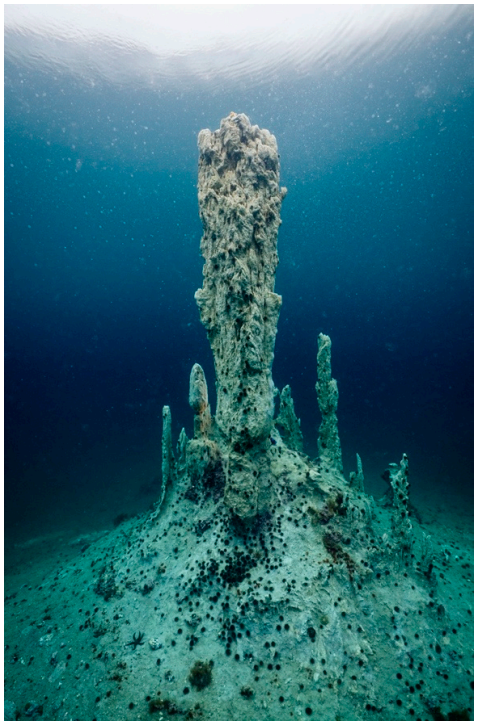


**Figure 3.** One group of the ikaite tufa columns of Ikka Fjord growing on top of a syenitic roches moutonneés. The tallest column in the centre is around 3.5 m tall. Photograph by Uli Kunz, SUBMARIS 2024.

The formation of natural ikaite is favoured by near-freezing temperatures, a high availability of alkaline earth metals and carbonate ions, and the presence of calcite inhibitors, like phosphate or $Mg^{2+}$, e.g., [2,30–32]. The hypothesis presented by Buchardt et al. (1997, 2001) [1,2] for the formation of ikaite in Ikka Fjord is that meteoric water generated by snow or rain percolates into the Grønnedal-Íka complex at the surface and passes through the lithological units of syenites and carbonatites. The initial solution of the groundwater is assumed to be pure meteoric water ($H_2O$) in equilibrium with atmospheric $CO_2$, which makes it slightly acidic (pH 5.6) and capable of dissolving minerals. A calcite-saturated brine produced by chemical weathering is released into springs at the foot of the mountains surrounding the fjord, whereas a different process, most likely from water–rock reactions deeper inside the complex, generates the alkaline groundwater that seeps up through fractures in the seabed of Ikka Fjord [1,2]. An elevation difference of c. 500 m from the top of the plateau to the seabed creates hydrostatic pressure that aids the seepage of fluids through sediment layers on the seabed. Thanks to the constant seepage of groundwater into seawater and the density differences between seawater and groundwater, ikaite tufa columns continuously grow upwards toward the sea surface at a growth rate of up to 0.5 m per year [3,26]. Ikka Fjord is the only place on Earth today where ikaite precipitates in the form of massive columns. Biological studies show that colonized microbes in the columns support their growth and promote their lifetime by protecting

them from corrosion by seawater, tides, and currents [33]. Ikaite is always present on Earth as a metastable mineral [34]; it starts to alter at temperatures above ~6 °C, by loss of $H_2O$ groups, into less hydrated calcium carbonate minerals of monohydrocalcite, aragonite, vaterite, and/or calcite, e.g., [4,5,35–37]. Arctic warming is believed to pose a threat to the temperature-sensitive ikaite columns. Air and seawater temperatures in the Arctic region are expected to increase markedly compared to the global average [38], and periods of seawater temperatures above 6 °C have already been detected in Ikka Fjord, resulting in mineral alterations and increased column fragility [5].

## 2. Material and Methods

### *2.1. Rock Samples and Analysis*

A total of 41 rock samples from the Grønnedal-Íka complex were collected during fieldwork in the summers of 2018 and 2019 by the geologists Gabrielle Stockmann, Eemu Ranta, Erik Sturkell, and Sigríður María Aðalsteinsdóttir. The majority were samples of nepheline syenites and various Gardar dykes in addition to five samples of carbonatites (e.g., the sample site shown in Figure 4). The samples were collected in the field using geological hammers, after which they were weighed and photographed for export. The export of samples has to be performed under a license issued by the Mineral License and Safety Authority (MLSA) in Greenland. Specifically, for this survey, the samples were exported under the Scientific Survey License nos. VU-00127 (2018) and VU-00154 (2019).

Out of the 41 rock samples, 24 were chosen for whole-rock analysis and thin-section preparation, based on the representation of the complex. The selected rock samples for this study were crushed using a jaw crusher, followed by grinding in an agate mortar to obtain <63 μm grain size for XRF analysis. Whole-rock chemical composition was determined on 24 samples in total, with a wavelength dispersive sequential X-ray spectrometer (Philips PW2404, Philips Analytical, Eindhoven, The Netherlands) fitted with a Rh anode end window X-ray tube, at the University of Edinburgh, and one sample (19SA29), with a WD-XRF (Axios FAST, PANalytical B.V., Almelo, The Netherlands) fitted with a range of anodes (Rh, Cr, Mo, Au), at ALS in Ireland. Both major (Si, Ti, Al, Fe, Mn, Mg, Ca, Na, K, P) and trace elements (Ba, Ce, Co, Cr, Cu, Ga, La, Nb, Ni, Rb, Sc, Sr, Rh, U, V, Y, Zr, Zn) were analysed.



**Figure 4.** An iron-rich carbonatite dyke intruded into a coarse-grained nepheline syenite (21FF245b, No 4 in Figure 2). Photograph by Erik Sturkell.

### *2.2. Chemical Analysis of Thin Sections*

A total of 24 thin sections were prepared for mineralogical inspection (Thin Section lab, Toulouse, France) and analysed using a polarizing microscope (Olympus BX51, equipped

with Olympus UC30 camera; Olympus Corporation, Tokyo, Japan). Three representative samples were selected to delineate unaltered rocks of the main lithologies: (1) nepheline syenite (18GS01), (2) calcio-carbonatite (18GS02), and (3) ferruginous carbonatite (19SA29) (see Figure 2 for sample locations). These were used for laboratory experiments and in geochemical modelling. Scanning Electron Microscopy (SEM) (Hitachi TM3000, Hitachi High-Technologies Corporation, Tokyo, Japan) analysis was carried out to estimate primary mineral abundances in BSE mode and with Gimp image software v. 2.10.16. The occurrence of primary mineral phases was confirmed with petrographic microscope inspection. The mineral compositions of both primary and secondary phases were determined using Electron Microprobe analysis (JEOL JXA-8230 SuperProbe, JEOL Ltd., Tokyo, Japan) equipped with a $LaB_6$ thermionic electron emitter at 15 keV voltage. The probe current was measured at the Faraday cup prior to each analysis. Opaque phases were identified with energy-dispersive spectroscopy (EDS). The current used varied depending on the minerals. Orthoclase, albite, and amphiboles were analysed with a beam current of 10 nA. Biotite, nepheline, sodalite, and calcite were analysed with a current of 5 nA, and pyroxenes were analysed with a current of 20 nA. REE and phosphate phases were determined with wavelength dispersive spectrometers (WDSs). The majority of the standards were provided courtesy of the Smithsonian Institution (NMNH and USNM standards) [39]. The CITZAF correction program [40] was used for all analyses, except for nepheline and sodalite, for which ZAF correction was applied.

### *2.3. Laboratory Experiments*

Six 150 mL bottle containers were used for batch experiments. Each bottle contained roughly 12 g of either crushed syenite (18GS01), carbonatite (19SA29), or a 50:50 mixture of syenite–carbonatite (around 6 g each) supplemented by 18 MQ DI water up until a final weight of 120 g. Three experiments were carried out at 20 ± 1 °C, and three experiments were carried out at 50 °C. Three containers were stored in a heating chamber at 50 °C, while the other three containers were stored in the laboratory area at ambient temperature. These were kept out of direct sunlight to avoid temperature fluctuations and the formation of organics. All bottles were shaken at regular intervals. Samples were collected every second day over a 10-day period. The pH of the samples was measured with a combined electrode calibrated with buffer solutions of pH 4, 7, and 10, with an accuracy of ±0.1 pH unit. The samples collected for major elements ($SiO_2$, Na, K, Ca, Mg, Fe, Al, B, $SO_4$) were filtered through a 0.2 µm cellulose acetate filter, acidified to 1% using $HNO_3$ (Merck Suprapur®, Merck KGaA, Darmstadt, Germany), and measured with inductively coupled plasma optical emission spectroscopy (ICP-OES, Thermo Scientific iCAP; Thermo Fisher Scientific Inc., Waltham, MA, USA), at the University of Iceland.

### *2.4. Geochemical Modelling*

Geochemical reaction path modelling was conducted to gain quantitative insight into the water–rock interaction processes and the formation of alkaline sodium bicarbonate–carbonate waters, which precipitates ikaite when mixed with seawater. Reaction path modelling is an effective and powerful geochemical tool to obtain insight into water–rock interactions and the mixing of waters. It can be used to simulate the weathering of rocks or water–rock interactions for the precipitation of certain minerals. The modelling considers the possible secondary phases and waters formed upon the dissolution of primary mineral phases, combined with a stepwise mixing of different fluids and the addition of gases. Geochemical reaction modelling is generally conducted as equilibrium reactions using thermodynamic data for 25 °C, which can be extrapolated to other temperatures. In this study, the modelling was carried out as equilibrium calculations with the aid of the PhreeqC

program v. 3.7 [41] using the carbfix.dat [42] and llnl.dat [43] databases extrapolated down to 5 °C. In the initial modelling, two different scenarios were considered: the first simulated an open system, where atmospheric $CO_2$ was allowed to equilibrate with the secondary waters formed during the modelling representing the formation of groundwater. The second simulated an open system where the secondary waters were cut off from atmospheric $CO_2$, illustrating the formation of surface waters.

Secondary minerals included in the geochemical calculations were selected among the common low-temperature weathering minerals of Al and Fe hydroxides, various smectites, kalsilite, chalcedony, and illite (Table 1). For the special case of Ikka Fjord, ikaite was also added [44]. The initial freshwater composition was taken to be the average rainwater of East Greenland [45]. The composition of the primary unaltered rocks was taken from the XRF analytical results of nepheline syenite (18GS01) and calcio-carbonatite (18GS02) (Table 2).

**Table 1.** Mineral–water reactions included in the geochemical calculations and their representative equilibrium constants at 25 °C.

| Mineral | Symbol | Equation | Dissolution Reaction | log K25 °C |
|---|---|---|---|---|
| *Primary phases* | | | | |
| Nepheline syenite | 18GS01 | $SiAl_{0.4074}Fe_{0.3649}Mg_{0.0165}Ca_{0.0426}Na_{0.2402}K_{0.1907}Mn_{0.0082}O_{3.288}$ | 18GS01 + 2.576$H^+$ = 0.4074$Al^{3+}$ + 0.0426$Ca^{2+}$ + 0.3064$Fe^{2+}$ + 0.0585$Fe^{3+}$ + 1.288$H_2O$ + 0.1907$K^+$ + 0.0165$Mg^{2+}$ + 0.0082$Mn^{2+}$ + 0.2402$Na^+$ + $SiO_2$ | undersat. [c] |
| Calcio-carbonatite | 18GS02 | $Fe_{0.009}Ca_1Mn_{0.003}C_{1.055}O_{3.122}$ | 18GS02 + 0.969$H^+$ + 0.043$H_2O$ = $Ca^{2+}$ + 0.009$Fe^{2+}$ + 1.055$HCO_3^-$ + 0.003$Mn^{2+}$ | undersat. [c] |
| Ferruginous calcio-carbonatite | 19SA29 | $SiAl_{0.04}Fe_{1.78}Mg_{0.05}Ca_{4.22}Na_{0.14}K_{0.01}Mn_{0.18}C_{3.97}O_{16.4}$ | 19SA29 + 8.95$H^+$ = 3.97$HCO_3^-$ + $SiO_2$ + 0.04$Al^{3+}$ + 1.59$Fe^{2+}$ + 0.19$Fe^{3+}$ + 0.05$Mg^{2+}$ + 4.22$Ca^{2+}$ + 0.14$Na^+$ + 0.01$K^+$ + 0.18$Mn^{2+}$ + 2.49$H_2O$ | undersat. [c] |
| *Secondary phases* | | | | |
| $Al(OH)_3$(am) | Al(am) | | | |
| Calcite | Cal | $CaCO_3$ | cal + $H^+$ = $Ca^{2+}$ + $HCO_3^-$ | 1.85 [a] |
| Celadonite | Cel | $KMgAlSi_4O_{10}(OH)_2$ | cel + 6 $H^+$ = $Al^{3+}$ + $K^+$ + $Mg^{2+}$ + 4$H_2O$ + 4$SiO_2$ | 7.46 [a] |
| Chalcedony | Cha | $SiO_2$ | cha = $SiO_2$ | −3.73 [a] |
| $Fe(OH)_3$ | $Fe(OH)_3$ | $Fe(OH)_3$ | $Fe(OH)_3$ + 3$H^+$ = $Fe^{3+}$ + 3$H_2O$ | 5.66 [a] |
| Gibbsite | Gbs | $Al(OH)_3$ | gib + 3$H^+$ = $Al^{3+}$ + 3$H_2O$ | 7.76 [a] |
| Goethite | Gth | FeOOH | goe + 3$H^+$ = $Fe^{3+}$ + 2$H_2O$ | 0.53 [a] |
| Illite | Ilt | $K_{0.6}Mg_{0.25}Al_{1.8}Al_{0.5}Si_{3.5}O_{10}(OH)_2$ | il +8$H^+$ = + 0.25 $Mg^{2+}$ + 0.60$K^+$ + 2.30$Al^{3+}$ + 3.50$SiO_2$ + 5$H_2O$ | 9.03 [b] |
| $Mn(OH)_2$(am) | Mn(am) | $Mn(OH)_2$ | $Mn(OH)_2$ + 2$H^+$ = $Mn^{2+}$ + 2$H_2O$ | 15.31 [a] |
| Montmorillonite-Ca | Mnt-Ca | $Ca_{.175}Mg_{.35}Al_{1.65}Si_4O_{10}(OH)_2$ | mon-ca + 6$H^+$ = 0.175$Ca^{2+}$ + 0.35$Mg^{2+}$ + 1.65$Al^{3+}$ + 4$H_2O$ + 4$SiO_2$ | 2.50 [a] |
| Montmorillonite-K | Mnt-K | $K_{.35}Mg_{.35}Al_{1.65}Si_4O_{10}(OH)_2$ | mon-k + 6$H^+$ = 0.35$K^+$ + 0.35$Mg^{2+}$ + 1.65$Al^{3+}$ + 4$H_2O$ + 4$SiO_2$ | 2.14 [a] |
| Montmorillonite-Mg | Mnt-Mg | $Mg_{.525}Al_{1.65}Si_4O_{10}(OH)_2$ | mon-mg + 6$H^+$ = 0.525$Mg^{2+}$ + 1.65$Al^{3+}$ + 4$H_2O$ + 4$SiO_2$ | 2.39 [a] |
| Montmorillonite-Na | Mnt-Na | $Na_{.35}Mg_{.35}Al_{1.65}Si_4O_{10}(OH)_2$ | mon-na + 6$H^+$ = 0.35$Mg^{2+}$ + 0.35$Na^+$ + 1.65$Al^{3+}$ + 4$H_2O$ + 4$SiO_2$ | 2.48 [a] |
| Nontronite-Ca | Non-Ca | $Ca_{.175}Fe_2Al_{.35}Si_{3.65}H_2O_{12}$ | mon-ca + 7.4$H^+$ = 0.175$Ca^{2+}$ + 0.35$Al^{3+}$ + 2$Fe^{3+}$ + 3.65$SiO_2$ + 4.7$H_2O$ | −11.58 [a] |
| Nontronite-K | Non-K | $K_{.35}Fe_2Al_{.35}Si_{3.65}H_2O_{12}$ | mon-k + 7.4$H^+$ = 0.35$Al^{3+}$ + 0.35$K^+$ + 2$Fe^{3+}$ + 3.65$SiO_2$ + 4.7$H_2O$ | −11.86 [a] |
| Nontronite-Mg | Non-Mg | $Mg_{.175}Fe_2Al_{.35}Si_{3.65}H_2O_{12}$ | mon-mg + 7.4$H^+$ = 0.175$Mg^{2+}$ + 0.35$Al^{+3}$ + 2$Fe^{3+}$ + 3.65$SiO_2$ + 4.7$H_2O$ | −11.62 [a] |
| Nontronite-Na | Non-Na | $Na_{.35}Fe_2Al_{.35}Si_{3.65}H_2O_{12}$ | mon-na + 7.4$H^+$ = 0.35$Al^{3+}$ + 0.35$Na^+$ + 2$Fe^{3+}$ + 3.65$SiO_2$ + 4.7$H_2O$ | −11.53 [a] |
| Saponite-Fe-Ca | Sap-Fe-Ca | $Ca_{.175}Fe_3Al_{.35}Si_{3.65}O_{10}(OH)_2$ | sap-fe-ca + 7.4$H^+$ = 0.175$Ca^{2+}$ + 0.35$Al^{3+}$ + 3$Fe^{2+}$ + 3.65$SiO_2$ + 4.7$H_2O$ | 20.36 [a] |
| Saponite-Fe-Fe | Sap-Fe-Fe | $Fe_{3.175}Al_{.35}Si_{3.65}O_{10}(OH)_2$ | sap-fe-fe + 7.4 $H^+$ = 0.35$Al^{3+}$ + 3.175$Fe^{2+}$ + 3.65$SiO_2$ + 4.7$H_2O$ | 18.94 [a] |
| Saponite-Fe-K | Sap-Fe-K | $K_{.35}Fe_3Al_{.35}Si_{3.65}O_{10}(OH)_2$ | sap-fe-k + 7.4$H^+$ = 0.35$K^+$ + 0.35$Al^{3+}$ + 3$Fe^{2+}$ + 3.65$SiO_2$ + 4.7$H_2O$ | 18.79 [a] |
| Saponite-Fe-Mg | Sap-Fe-Mg | $Mg_{.175}Fe_3Al_{.35}Si_{3.65}O_{10}(OH)_2$ | sap-fe-mg + 7.4$H^+$ = 0.175$Mg^{2+}$ + 0.35$Al^{3+}$ + 3$Fe^{2+}$ + 3.65$SiO_2$ + 4.7$H_2O$ | 19.53 [a] |
| Saponite-Fe-Na | Sap-Fe-Na | $Na_{.35}Fe_3Al_{.35}Si_{3.65}O_{10}(OH)_2$ | sap-fe-na + 7.4$H^+$ = 0.35$Na^+$ + 0.35$Al^{3+}$ + 3$Fe^{2+}$ + 3.65$SiO_2$ | 19.80 [a] |
| Kalsilite | Kls | $KAlSiO_4$ | kal + 4H+ = $Al^{3+}$ + $K^+$ + $SiO_2$ + 2$H_2O$ | 10.90 [a] |
| Ikaite | Ika | $CaCO_3 \cdot 6H_2O$ | ika + H+ = $Ca^{2+}$ + 6$H_2O$ + $HCO_3^-$ | 2.87 [d] |

[a] carbfix.dat [42], [b] llnl.dat [43], [c] this study (logK25 °C set to undersaturation) and [d] Krupka et al. (2010) [44].

**Table 2.** Starting water composition and rock composition used for geochemical modelling.

| Type of Water | Area | Locality | Temp | pH | $H^+$ | $Na^+$ | $K^+$ | $Ca^{2+}$ | $Mg^{2+}$ | $Cl^-$ | $NH_4^-$ | $NO_3^-$ | $SO_4^-$ | | |
|---|---|---|---|---|---|---|---|---|---|---|---|---|---|---|---|
| Average rainwater composition from E Greenland [45]. | Mestersvig | AGA site at Mestersvig airfield | 5 °C | 5.6 | 0.01 | $1.05 \times 10^{-3}$ | $1.05 \times 10^{-3}$ | $4.37 \times 10^{-3}$ | $4 \times 10^{-3}$ | $1.13 \times 10^{-2}$ | $8.29 \times 10^{-3}$ | $9.44 \times 10^{-3}$ | $1.054 \times 10^{-2}$ | | |
| **Rock composition** | | | | | **$SiO_2$** | **$Al_2O_3$** | **$Fe_2O_3$** | **MgO** | **CaO** | **$Na_2O$** | **$K_2O$** | **$TiO_2$** | **MnO** | **$P_2O_5$** | **Loi** | **Total** |
| Calcio-carbonatite 18GS02 | Ikka fjord | Grønnedal–Íka | | | N.D. | N.D. | 1.17 | N.D. | 54.91 | N.D. | N.D. | 0.001 | 0.178 | N.D. | 43.6 | 99.86 |
| Nepheline Syenite 18GS01 | Ikka fjord | Grønnedal–Íka | | | 53.21 | 19.14 | 9.07 | 0.68 | 1.48 | 8.55 | 5.713 | 0.374 | 0.262 | 0.134 | 1.36 | 99.97 |

## 3. Results

### *3.1. Whole Rock Composition and Mineralogy*

A total of 24 samples were analysed for major and minor chemical composition. By the aid of a petrographic microscope, the least altered samples were chosen for further studies based on their mineral chemistry and primary phase abundances. The major and minor element compositions of the 24 rock samples are listed in Supplementary Material Table S1. The primary mineral compositions obtained with EMPA are provided in Table 3, and the total EMPA analysis, with secondary minerals, is provided in Supplementary Material Tables S2 and S3.

The compositions of all the syenite and carbonatite samples described in this study are shown in Figure 5. The majority of the analysed syenites are plotted as foid syenite, including sample 18GS01, chosen as representative of an unaltered syenite (Figure 5a). A few samples are classified as either foidolite, foid monzosyenite, or syenite (Figure 5a). The foid syenites are the most alkaline, with $Na_2O + K_2O$ in the range of 13–16 wt%, whereas the foid monzosyenites have lower alkalis of 11–12 wt%. Most of the samples have an intermediate silica content, except for the two more felsic samples, which are classified as syenites. The nepheline syenites can be divided into three groups: (1) coarse-grained, (2) fine-grained and micro-syenites, and (3) syenites with pyroxene as a primary mineral, in agreement with previous studies, e.g., [8]. The analysed nepheline syenites have undergone various degrees of alteration, from mild alteration of the rim of the primary minerals to almost complete pseudomorphic replacement by alteration minerals.

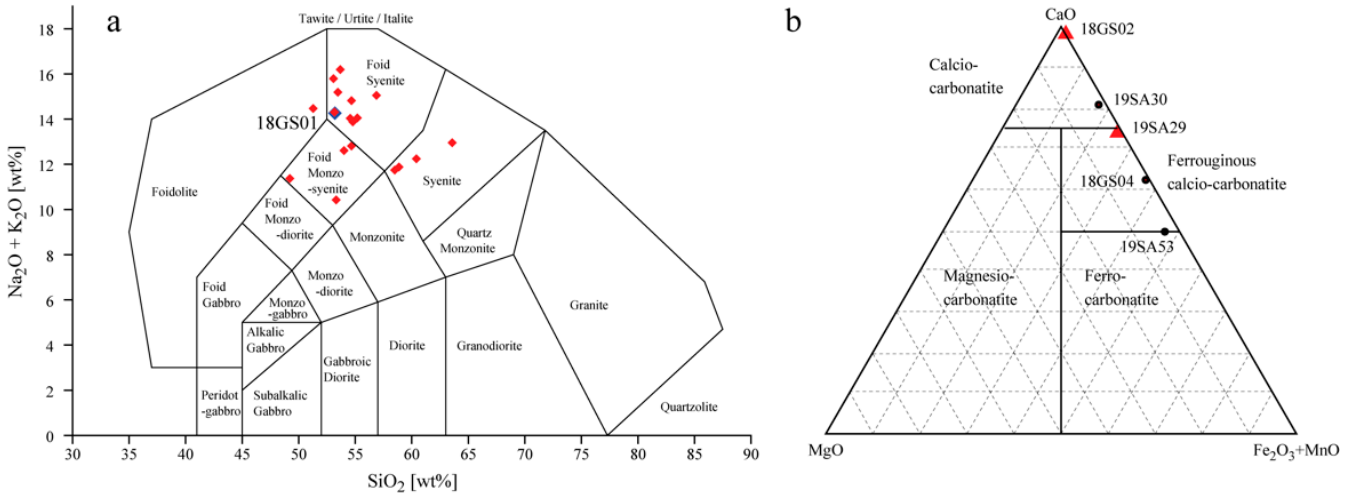



**Figure 5.** (**a**) Total alkali-silica (TAS) classification scheme after Middlemost (1994) [46]. Syenite samples are plotted as foid monzosyenite, foid syenite, and syenite. Sample 18GS01, marked as blue diamond, is classified as foid syenite. The red diamonds are other syenite samples analysed for whole-rock chemistry (**b**) Carbonatite classification diagram based on CaO, MgO, and $Fe_2O_3$ + MnO contents, after Gittins and Harmer (1997) [47]. Values are shown as mol%, and the compositional fields of different carbonatites are indicated: calcio-carbonatite, magnesio-carbonatite, ferruginous calcio-carbonatite, and ferro-carbonatite. Red triangles are samples that were looked at in more detail and blue circles other samples analysed for whole-rock chemistry.

**Table 3.** Mineral chemistry and relative abundance of primary minerals in wt%. EMPA analysis for minerals is given in S2, and REE and fluorite phases (<1 wt%) are given in S3.

| | Nepheline Syenite (18GS01) | | | | | | | |
|---|---|---|---|---|---|---|---|---|
| | **Or (28%)** | **Ab (24%)** | **Nph (25%)** | **Aeg-Aug (6%)** | **Bt** | **Rbk (2%)** | **Frct (2%)** | **Ap (1%)** |
| $SiO_2$ | 64.17–65.72 | 68.09–69.11 | 43.02–45.07 | 49.94–52.09 | 34.20–35.50 | 51.33–55.61 | 50.73 | 0–0.58 |
| $TiO_2$ | 0–0.03 | 0–0.02 | 0–0.02 | 0.17–0.61 | 1.84–2.91 | 0.17–0.2 | 0.14 | |
| $Al_2O_3$ | 18.44–18.96 | 19.54–20.28 | 32.62–33.65 | 0.84–2.05 | 11.85–13.12 | 0.45 | 1.23 | |
| $Cr_2O_3$ | | | | 0–0.02 | | | | |
| FeO | 0.10–0.31 | 0.08–0.49 | 0.54–0.94 | 6.72–9.20 | 8.39–10.59 | 20.01–20.43 | 28.41 | |
| $Fe_2O_3$ | | | | 20.43–23.30 | 24.16–28.06 | 17.48–18.08 | | |
| MnO | 0–0.02 | 0–0.04 | | 0.53–0.94 | 1.20–1.38 | 0.09–0.6 | 0.6 | |
| MgO | 0–0.02 | 0–0.02 | 0–0.03 | 0.55–1.52 | 1.96–5.55 | 1.77–1.79 | 0.7 | |
| CaO | 0–0.01 | 0–0.25 | 0–0.05 | 4.59–7.31 | 0–0.08 | 0.40–0.44 | 6.93 | |
| BaO | 0–0.21 | 0–0.02 | | | | | | |
| $P_2O_5$ | | | | | | | | 40.35–45.41 |
| $Na_2O$ | 0.37–1.26 | 10.33–11.46 | 15.04–15.60 | 8.94–10.44 | 0–0.27 | 6.63–6.67 | 9.28 | 0.23–0.74 |
| $K_2O$ | 15.19–16.72 | 0.04–0.18 | 5.54–6.62 | | 8.83–9.36 | 0.07–0.08 | 0.01 | |
| SrO | | | 0–0.05 | | | | | |
| $La_2O_3$ | | | | | | | | 0–1.56 |
| $CeO_2$ | | | | | | | | 0.85–2.44 |
| F | | | | | 0–0.28 | | | 5.26–9.33 |
| Cl | | | | | 0–0.01 | | 0.002 | |

| | **Carbonatite (19SA29)** | | **Carbonatite (18GS02)** |
|---|---|---|---|
| | **Cal (64%)** | **Ank (10%)** | **Rbk (8%)** | **Cal (99%)** |
| $SiO_2$ | | | 50.65–51.86 | |
| $TiO_2$ | | | 0.10–1.05 | |
| $Al_2O_3$ | | | 0.34–0.75 | |
| FeO | 0.57–3.87 | 18.26–19.23 | 19.21–21.18 | 0.74–1.38 |
| $Fe_2O_3$ | | | 16.50–18.33 | |
| MnO | 0.93–5.59 | 0.73–1.22 | 0.02–0.11 | 0.01–0.48 |
| MgO | 0.09–0.18 | 6.06–7.70 | 1.49–2.32 | 0–0.12 |
| CaO | 42.02–52.54 | 23.79–27.72 | 0.06–0.66 | 52.01–54.14 |
| $Na_2O$ | | | 6.32–6.79 | |
| $K_2O$ | | | 0.07–0.19 | |

**Table 3.** *Cont.*

| | Carbonatite (19SA29) | | Carbonatite (18GS02) | |
|---|---|---|---|---|
| | **Cal (64%)** | **Ank (10%)** | **Rbk (8%)** | **Cal (99%)** |
| $Cr_2O_3$ | | | 0–0.02 | |
| NiO | | | 0–0.04 | |
| SrO | 0–0.13 | 0.34–0.53 | | 0.27–0.98 |
| BaO | 0–0.13 | 0.01–0.05 | | 0–0.07 |
| $CO_2$ | 43.70–51.91 | 44.61–48.50 | | 44–45.90 |

Mineral abbreviations: orthoclase: Or, albite: Ab, nepheline: Nph, aegirine–augite: Aeg-Aug, biotite: Bt, riebeckite: Rbk, ferro-richterite: Frct, apatite: Ap, calcite: Cal, and ankerite: Ank.

Sample 18GS01 (Figure 6a), selected for experiments and modelling, is the least altered and belongs to the nepheline syenite group that includes pyroxene. The sample consists of large, up to 1.5 cm elongated K-feldspars (28 vol%) and albite (24 vol%) with a perthite structure and exsolution lamellae of orthoclase (Or) and albite (Ab) (Figure 6a). As illustrated in Figure 6b, the second most common phase in the sample is relatively unaltered nepheline (25 vol%), generally occurring as 3 mm sized grains. Mild alteration is observed along the rims of nepheline crystals. Based on the study by Tollefsen et al. (2019) [6], the alteration mineral is likely cancrinite ($Na_7Ca[Al_6Si_6O_{24}](CO_3)_{1.5}\bullet 2H_2O$). Pyroxenes (6 vol%), amphiboles (4 vol%), and biotite (1 vol%) are observed both as individual crystals and as intergrowths with K-feldspars and feldspathoids. Albite rims around orthoclase crystals generally have pyroxenes or biotite inclusions.

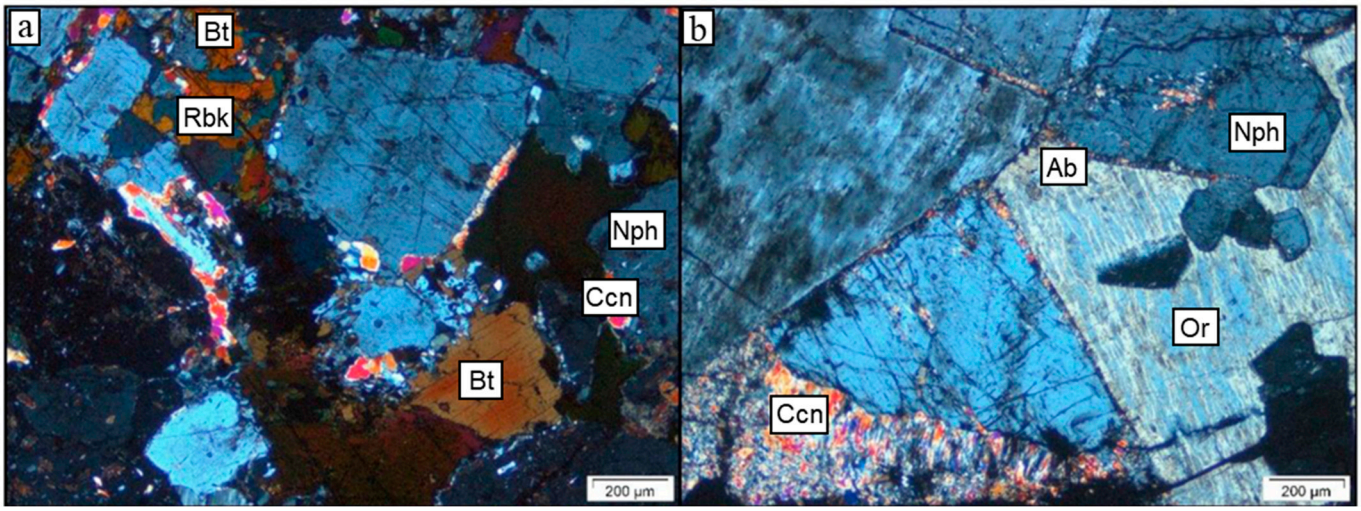



**Figure 6.** Photomicrograph of the nepheline syenite samples from the 2018 and 2019 fieldwork. (**a**) (XPL): Sample 18GS01, the least altered sample. The alteration is likely high-T cancrinite (ccn) alteration at the rim of the nepheline (nph) grain. Grains of biotite (bt) and riebeckite (rbk) are also shown. (**b**) (XPL): Sample 19SA68D, an example of extensive alteration between feldspar grains with both albite (ab) and orthoclase (or) of nepheline grains and interstitial alteration minerals of possible cancrinite (ccn).

Most of the inclusions within the pyroxenes are REE minerals, and the rims of the grains are relatively unaltered (Figure 6a). In summary, based on the petrographic results, the primary minerals in sample 18GS01 (Figure 6a) (volume%) are orthoclase ($KAlSi_3O_8$) (28%), albite ($NaAlSi_3O_8$) (24%), nepheline ($(Na,K)AlSiO_4$) (25%), aegirine–augite.

$(NaCaFe^{2+}Mg)(Fe^{3+}AlFe^{2+}Mg)Si_2O_6$) (6%), riebeckite ($[Na_2][Fe^{2+}{}_3Fe^{3+}{}_2]Si_8O_{22}(OH)_2$) (2%), ferro-richterite ($\{Na\}\{CaNa\}\{Fe^{2+}{}_5\}(Si_8O_{22})(OH)_2$) (2%), biotite ($K(Mg,Fe)_3AlSi_3O_{10}(F,OH)_2$) (1%), apatite ($Ca_5(PO_4)_3(F,Cl,OH)$) (1%), columbite ($(Fe^{2+},Mn)(Nb,Ta)_2O_6$), Y-Ce pyrochlore $(Na, Ca)_2Nb_2O_6(OH,F)$, zircon ($ZrSiO_4$), and unknown F-rich minerals) (1%). The mineralogy of the remaining volume is unaccounted for, as those minerals were not considered primary phases.

The XRF results of the carbonatite samples identify them as either Ca-rich calcio-carbonatite or Fe-rich ferruginous calcio-carbonatite and ferro-carbonatite (Figure 5b). Figure 4 illustrates a Fe-rich carbonatite dyke cutting through a coarse-grained syenite in the Grønnedal-Íka complex. Two carbonatites were chosen for further studies: (1) calcio-carbonatite (18GS02, Figure 7b), composed mainly of calcite (99%) and minor F-rich minerals (1%), e.g., REE-enriched varieties of fluorite ($CaF_2$), and (2) a ferruginous calcio-carbonatite (19SA29, Figure 7a) with an unusual mineral assemblage of calcite (64%), ankerite (10%), riebeckite (8%), and F-rich minerals (1%). The EDS measurements con-

firmed phases of the REE-enriched minerals knopite ((Ca,Ce,Na)(Ti,Fe)$O_3$) and monazite (REE($PO_4$)) in 19SA29 and yttrocerite ((Ca,Y,Ce)$F^{2+}{}_x$) in 18GS02. Bluish to black grains of the amphibole riebeckite enclosed in calcite minerals are easily visible in the hand specimen and thin section of sample 19SA29 (Figure 7a). Amphiboles are rare in carbonatites [48], and riebeckite has not been described before in a carbonatite from the Grønnedal-Íka complex, e.g., [23,24,49]. This makes sample 19SA29 an interesting specimen to study further. The backscattered electron images and photomicrographs show the fibrous structure of riebeckite within calcite and ankerite (Figure 7a). Calcite occurs either as up to 1 cm long grains between crystals of riebeckite or as smaller mm-sized grains interstitial between riebeckite crystals. Fibrous iron oxide minerals are interstitial between riebeckites. The sample represents a smaller intruding body of carbonatite into the gneissic host rock, and the thin section includes the carbonatite–gneiss contact. A minor amount of quartz ($SiO_2$) was detected close to the contact.

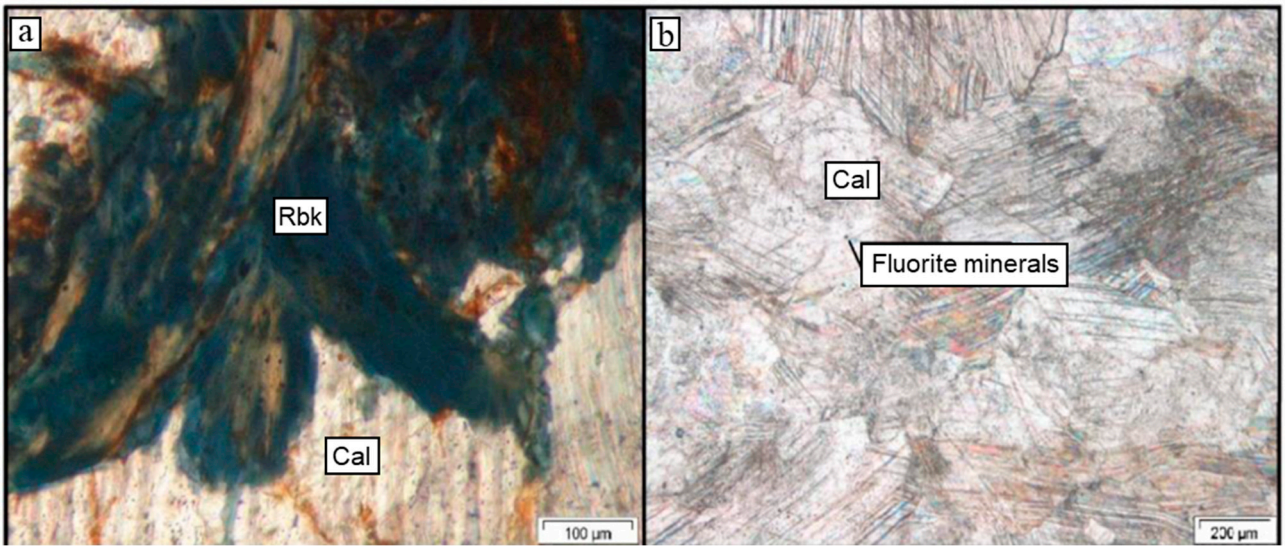



**Figure 7.** Photomicrographs of carbonatite samples. (**a**): (PPL) Blue, fibrous riebeckite (rbk) and iron oxide mineral in 19SA29. (**b**): (PPL) Sample 18GS02, consisting mainly of calcite (cal).

### *3.2. Laboratory Experiments*

Figure 8 depicts the pH results of the six batch experiments containing either (1) nepheline syenite (18GS01), (2) carbonatite (19SA29), or (3) a 1:1 mixture of syenite and carbonatite at 20 (Figure 8a) and 50 °C (Figure 8b). At both temperatures, the pH of the solution in contact with crushed syenite rises sharply to a pH $\geq$ 10 and reaches a steady state around pH 10.

In contrast, the solution in contact with crushed carbonatite of dominantly calcite composition reaches a steady state around pH 8. The 1:1 mixtures of nepheline syenite and carbonatite show more fluctuating pH values with the experiment at 20 °C, ending up around pH 8 close to the pH value of carbonatite, whereas the experiment at 50 °C reaches a steady state at pH 8.6. All pH results and ICP-OES analysis are provided in Supplementary Material, Table S4.

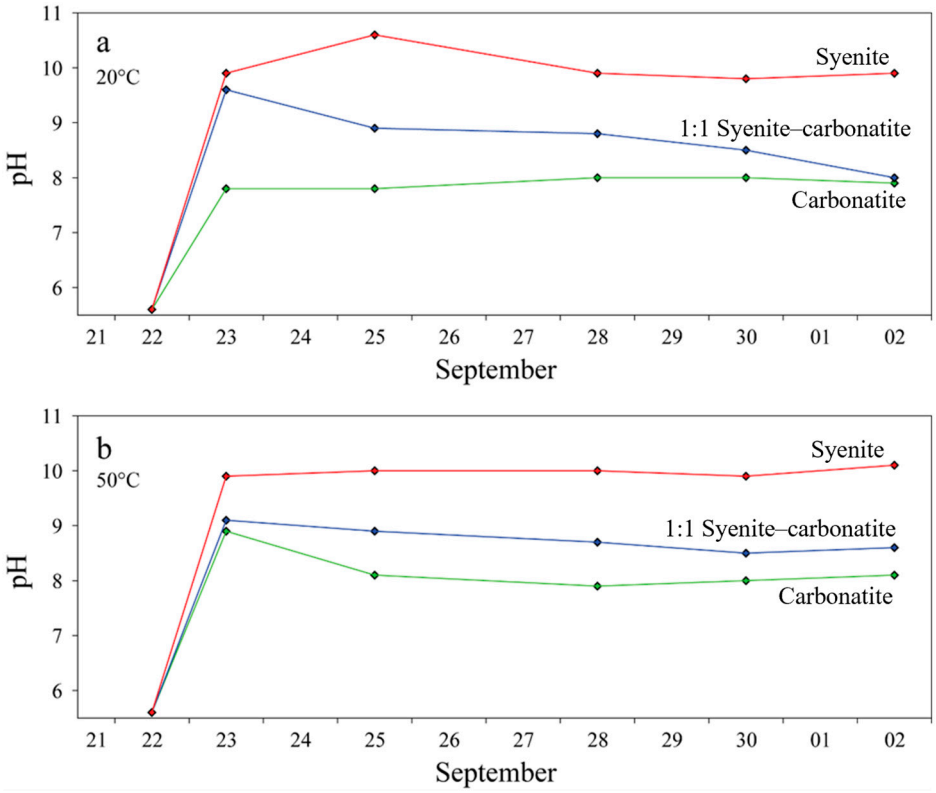



**Figure 8.** The change in pH with time results of in-batch experiments of syenite, carbonatite, and a mixture at 20 °C (**a**) and 50 °C (**b**) (pH = 5.6 at t = 0).

### *3.3. Geochemical Modelling*

The modelling provides results of the water composition and speciation at equilibrium and the secondary mineral formation at saturation upon the low-temperature weathering of the rocks selected. Progressive water–rock interactions were simulated and measured as the amount (mol) of rock dissolved in a kg of water (R/W ratio). The starting point for the water composition used in the calculations was that of rainwater collected from E Greenland [45] (Table 2). As primary solid phases, the calculated bulk chemical compositions for nepheline syenite (18GS01) and calcio-carbonatite (18GS02) were used and dissolved stoichiometrically (Table 1). The secondary solid phases used in the simulation were the common low-temperature weathering minerals of (Fe, Al) oxides, (Fe, Na, Ca, K) smectite group clays, kalsilite, illite, chalcedony, and, in addition, either calcite or ikaite. Simulations of an open system (a) and a closed system (b) with respect to atmospheric $CO_2$(g) were run as a 1:1 mixture of nepheline syenite and calcio-carbonatite (exp. 1) and as a 1:1 mixture of nepheline syenite and ferruginouscarbonatite (exp. 2) at three different molar solutions for the water–rock titration, at 0.001, 0.01, and 1 molar, over 100 steps each. The equilibrium phases chosen for the modelling are listed in Table 1, and the results are plotted in Figures 9 and 10.

The reaction path modelling of nepheline syenite mixed 1:1 with either calcio-carbonatite or ferruginous carbonatite shows the simultaneous precipitation of calcium carbonate minerals (e.g., calcite or ikaite), amorphous manganese oxide, smectite, illite, kalsilite, alumina oxide, and, in the ferruginous system, goethite. Simple oxides form early, followed by clays and $CaCO_3$ minerals, depending on the chosen carbonate phase.

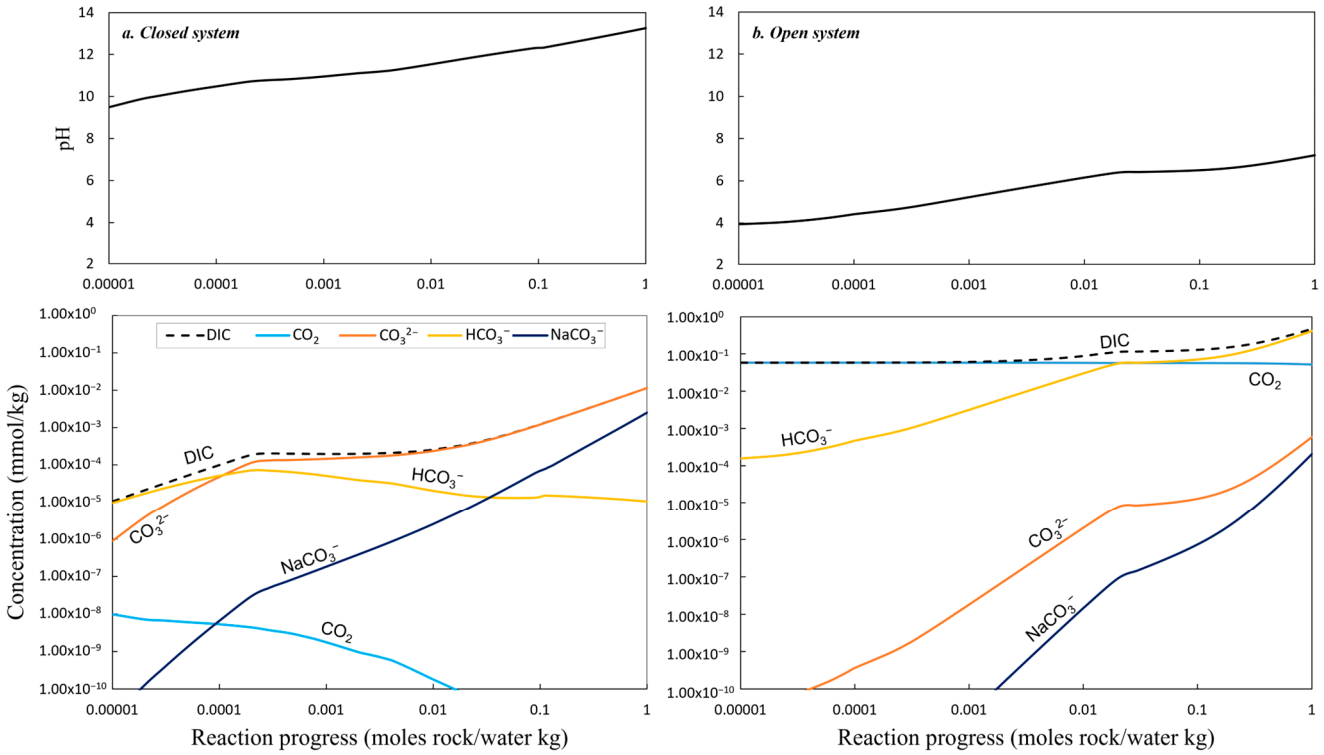



**Figure 9.** The top row depicts the simulated pH variation in the secondary fluids at 5 °C as a function of the reaction progress (rock mol/water kg). The lower row depicts the concentration in mmol/kg of major dissolved inorganic carbon (DIC) species in the secondary fluids as a function of the reaction progress in a closed system (**a**) and an open system (**b**).

For the closed system (b), excluding atmospheric $CO_2$, the initial pH of 9.5 rises to 13.5 (Figure 9a), with ikaite, gibbsite, $Mn(OH)_2$, illite, and smectite precipitating (Figure 10a). The dominant Ca species is $CaCO_3$(aq), with high Na+ and DIC but low $CO_2$ at pH > 10.5. Over time, ikaite saturation increases alongside gibbsite, $Mn(OH)_2$, kalsilite, chalcedony, and saponite-Na.

In the open system (a), where atmospheric $CO_2$ equilibrates, the pH starts at 4 and stabilizes at 7. The primary DIC species shift to $CO_2$(aq) and $HCO_3^-$(aq) (Figure 9b), with calcite, gibbsite, and smectite precipitating above pH 6.5. Chalcedony forms under acidic conditions, and high Ca concentrations persist until pH 6.5, after which $CO_2$(aq), $Na^+$, and $K^+$ dominate the fluid chemistry.

Using ferruginous carbonatite (19SA29) in exp. 2 resulted in a slightly higher initial pH (10.5–13.5), with continuous goethite precipitation. Aqueous species were alike to exp. 1, except $Ca^{2+}$ replaced $CaCO_3$(aq) as the dominant calcium species, and $Ca^+$ was equal to $Na^+$ in concentration. The effects of more Fe-rich carbonatite dissolution were not examined. Including analcime in the simulations significantly reduced the $Na^+$ concentrations, consistent with the pseudomorphic replacement of nepheline by analcime and illite, as suggested by Tollefsen et al. (2019) [6]. Using calcite instead of metastable ikaite led to ikaite undersaturation due to calcite's greater thermodynamic stability.

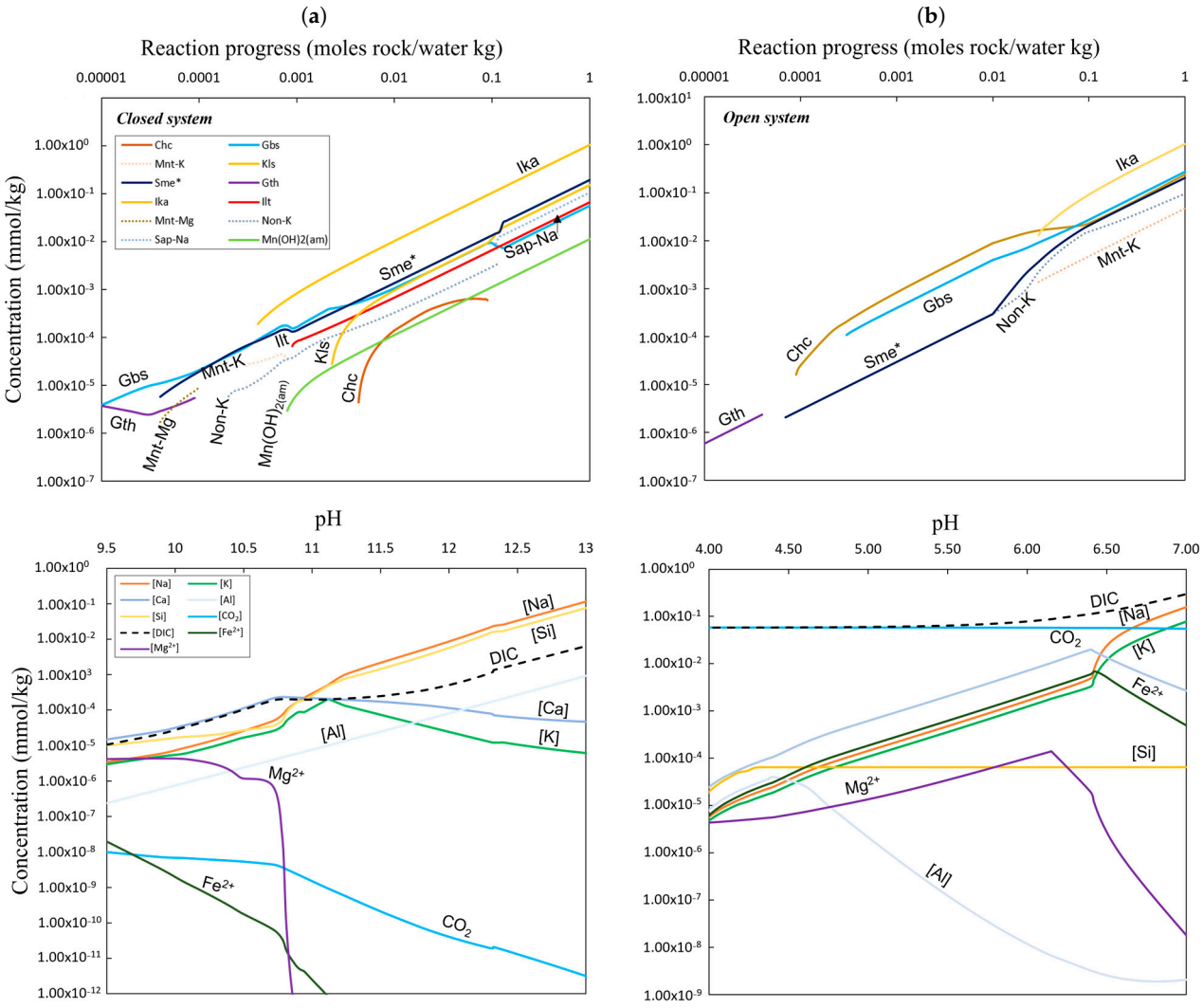



**Figure 10.** The top row illustrates the simulated phase assemblage of the secondary minerals formed at 5 °C as a function of the reaction progress from a starting material containing a 1:1 ratio of nepheline syenite and calcio-carbonatite for a closed system (**a**) and an open system (**b**). Sme* represents the sum of sub-groups of smectite clay (nontronite, saponite, and montmorillonite). The lower row depicts the simulated concentrations of the major ions and the most important total elements (Σ) (mmol/kg) of the secondary fluids as a function of pH at 5 °C. Elements with a concentration lower than $\times 10^{-10}$ (mmol/kg) are not included in the graph ($Fe^{3+}$). Mineral abbreviations: ikaite: Ika, gibbsite: Gbs, goethite: Gth, smectite: Sme, montmorillonite-K: Mnt-K, montmorillonite-Mg, nontronite-K: Non-K, kalsilite: Kls, chalcedony: Chc, saponite-Na: Sap-Na, and illite: Ilt.

## 4. Discussion

The laboratory batch experiments show that the high pH (>10) mainly arises from the dissolution of nepheline syenite, which releases $Na^+$ ions into solution. This increase in pH likely results from cation exchange, where $Na^+$ replaces $H^+$ on mineral surfaces, and possibly also from the hydrolysis of aluminosilicates, both of which consume protons and elevate the pH. This interpretation aligns with the results of Tollefsen et al. (2019) [6]. Surprisingly, the pH of the batch solution responds within one day to dissolving ions both at 20 and 50 °C (Figure 8), which points to an easy exchange of $Na^+$ with $H^+$ in the sodium-bearing minerals, e.g., nepheline [50]. The dissolution of calcio-carbonatite in the batch experiments reached a steady-state pH of 8 in the solutions at both experimental temperatures. This pH corresponds to the solution sitting at calcite saturation and fits well with calcite being the main mineral component of the selected rock sample. Based on these

experimental results, the dissolution of nepheline syenite is the main driver of the observed high pH of 9.5–11 found in the natural column water of Ikka Fjord [2,51], keeping in mind that natural systems may respond slower, e.g., due to lower temperatures (3–4 °C).

The PhreeqC geochemical modelling results indicate that the groundwater itself becomes saturated in ikaite. The precipitation of ikaite within the column water is controlled by the availability of calcium ions from the groundwater, not the seawater, in this case. The mixing of groundwater with seawater leads to an even higher degree of supersaturation with respect to calcium carbonate minerals. However, according to the modelling, the availability of calcium and carbonate ions is high enough in the groundwater to reach saturation of ikaite on its own, and the cold climate aids the stability of the metastable mineral. This observation fits the modelling results of Stockmann et al. (2018) [31], who modelled the chemistry of real column water sampled from two column areas in Ikka Fjord, 'the Atoll' and 'Lejrfeltet' (see Figure 2), at a near in situ temperature of 5 °C. The Atoll column water was saturated with respect to ikaite, whereas Lejrfeltet was slightly undersaturated [31]. This means the groundwater itself could provide the seed crystals for ikaite in the sediments on the seabed of Ikka Fjord, ensuring the starting points for column growth.

With respect to chemical weathering reactions of the nepheline syenites and carbonatites, there are no experiments from the literature for comparison. The main sources for comparison are the endmember compositions of the fluids sampled from columns, rivers, streams, and the lakes of Ikka Fjord [2,27,31] and a study of rock alteration in the Grønnedal-Íka complex [26]. Therefore, the selected phase assemblage for the modelling cannot be confirmed by methods other than laboratory experiments and by a detailed study of mineral weathering in the rocks of the Grønnedal-Íka complex. Nevertheless, the PhreeqC model gives a good overview of the major species in the system, with probable secondary solid phases forming and fluid chemistry. Keeping in mind this simplification of the system, the main equilibrium phases formed are simple oxides, various clay minerals, and carbonate minerals, which can either be calcite, ikaite, or other calcium carbonate minerals (e.g., monohydrocalcite or aragonite), depending on which one is chosen in the model run. Iron-rich carbonatites are also common in the Grønnedal-Íka complex and are shown to oxidize to magnetite, hematite, or Fe hydroxides, depending on the redox conditions [21,23]. Therefore, these will also contribute bicarbonate and carbonate ions to the column water (but not Fe) [6]. The concentrations of $Mg^{2+}$ and $Fe^{2+}$ decrease with increasing pH, likely due to the precipitation of hydroxides (e.g., brucite for $Mg^{2+}$), which are favoured by an alkaline pH and low temperatures, as well as possible iron carbonate minerals (e.g., siderite), and the formation of other clay minerals shown in the model. A low $Ca^{2+}$ concentration of 0.17 mmol/kg in the real column water [1], and with the above modelling results at hand, implies that primary carbonates of calcite and siderite are dissolved by the slightly acidified groundwater entering the Grønnedal-Íka complex. This, in turn, leads to the precipitation of secondary calcium-containing minerals and, thus, the low concentration of observed $Ca^{2+}$ in the natural fluids. Parameters that could favour ikaite precipitation within the igneous complex are, e.g., high pH, low water temperature, and the presence of phosphate from dissolved apatite acting as an inhibitor of calcite [2]. It should be noted that the existence of easily dissolved sodium–calcium carbonates of, e.g., pirssonite ($Na_2Ca(CO_3)_2 \cdot 2H_2O$) and gaylussite ($Na_2Ca(CO_3)_2 \cdot 5H_2O$) have also been suggested to exist inside the complex [2]. The next question would be if any of these chemical reactions are exothermic to a degree that could explain the homeothermic springs of 4 °C running only at the foot of the carbonatite intrusion and not in the nepheline syenite areas. For comparison, a study on the self-healing properties of ancient Roman cement shows how an initial process of hot mixing between water and lime (CaO) creates extensive

exothermic energy and forms $CaCO_3$ crystals in the cement matrix through the carbonation of an original CaO clast [52]. These will dissolve and re-precipitate upon crack formation and water interaction, and the identity of the $CaCO_3$ mineral can vary from calcite to aragonite, vaterite, or amorphous $CaCO_3$, depending on the degree of hydration [52].

The real column water of Ikka Fjord has a potassium concentration of 1.9 mmol/kg [1], and K-rich secondary mineral phases must be included in the modelling to lower the potassium concentration in the secondary fluids to match this fluid chemistry. One way to circumvent the potassium problem is to include the feldspathoid kalsilite ($KAlSiO_4$) in the modelling, which is the K-endmember of nepheline. If kalsilite is excluded from the modelling, the simulated solid phases and the major fluid components are identical to the modelling, except for the concentration of $K^+$, which increases and matches the high concentration of $Na^+$. Thus, the measured low K concentration of the column water indicates there must be a secondary K-bearing phase, like kalsilite, or other phases of, e.g., zeolites or feldspar alteration that use up the potassium.

The modelling shows that groundwater fluids corresponding to the real column water with high concentrations of $Na^+$ and DIC species can indeed be generated from the water–rock interaction of nepheline syenite and calcio-carbonatite under the following conditions: (1) a closed system and (2) when (Fe, Al, Mn) oxides, (Fe-Na, Fe-K, Fe-Mg, Fe-Fe, Mg, Na, K) the smectite group, and (K-Mg) illite clays, kalsilite, and calcium carbonates are allowed to precipitate. Clays do not consume $K^+$ or $Na^+$ to a great extent; therefore, other mineral phases, like kalsilite, must be included to reduce the concentrations of $K^+$. The major aqueous species of the secondary fluids produced by simulating the dissolution of a 1:1 mix of nepheline syenite and calcio-carbonatite are $Na^+$, $CO_3^{2-}$, $HCO_3^-$, and $NaCO_3$(aq). The $NaCO_3$(aq) ion species is generally considered to exist in minor concentrations in earth systems [53], but it is one of the major species, according to the modelling results, of the simulated system.

The isotopic and chemical composition of the seawater in Ikka Fjord and the composition of the surface waters are significantly different from the water seeping from the columns [2,27] (Table 4). Subaerial springs along the west side of the fjord are slightly elevated in alkalinity and Ca concentrations, leading to calcite saturation and pH 8, but these springs lack the high concentrations of sodium and carbonates characteristic of the column water [1,2]. The likely confined aquifer below the seabed is sealed off by a compact layer of glaciomarine clay and is likely fed by groundwater draining from the mountains surrounding the fjord [3,54] This indicates that the alkaline waters are more likely to be generated in conditions where the water is not in equilibrium with atmospheric $CO_2$(g), in correspondence with the best-fit modelling in this work. Overall, the concentrations and speciation of elements obtained with the simulations under closed system conditions correlate well with what has been analysed in Ikka Fjord. The column water sampled from the Atoll column has a pH of 10.6 (at 4 °C) and a $Na^+$ concentration of 190 mmol/kg [2]. In the modelling, the highest concentration of $Na^+$ in the simulated fluids is reached at pH 13.5 (at 5 °C) with 219 mmol/kg. The fluids are rich in dissolved inorganic carbon, and the major aqueous species are $Na^+$, $CO_3^{2-}$, $HCO_3^-$, and $NaCO_3$(aq), which is identical to the real column water [2]. Calcium ions are mainly present as $CaCO_3$(aq) and not as $Ca^{2+}$ ions, again correlating well with studies of the column water [2,31]. The total $CO_2$ is $1.052 \times 10^{-2}$ mmol/kg in the initial stage of the reaction and $8.435 \times 10^{-2}$ mmol/kg at the end of the simulation for a closed system. In comparison, Buchardt et al. (2001) [2] calculated the $CO_2$ concentration of the column water as $3 \times 10^{-3}$ mmol/L, which is equal to a $CO_2$ partial pressure of $0.04 \times 10^{-3}$ bar.

If kinetic parameters were included in the modelling, the major ion chemical composition would likely be identical to the solution chemistry modelled here. However,

reaction kinetics may inhibit or slow reactions, like in the present case of Ikka Fjord, where metastable ikaite, monohydrocalcite, and aragonite form instead of thermodynamically more stable calcite [2,5,35]. The precipitation of ikaite in a cold marine environment is kinetically favoured because $Mg^{2+}$ in seawater inhibits the growth of calcite [32] and due to the water becoming more saturated with respect to ikaite with decreasing temperature, in contrast to the dehydrated $CaCO_3$ minerals [31]. This favours ikaite precipitation at water temperatures close to 0 °C [30], keeping in mind that trace amounts of monohydrate, calcite, and aragonite have been identified in the columns [5]. Although the geochemical program PhreeqC is a powerful tool to model reactions, it is equilibrium-based and assumes instantaneous chemical equilibrium for all reactions, which is seldom the case in nature and is limiting for metastable phases, such as ikaite and monohydrocalcite. Reaction rates, kinetic barriers, and transport processes significantly affect mineral precipitation and dissolution pathways [55]. Weathering reactions in nature are often non-stochiometric, leading to preferential leaching or selective dissolution of ions from minerals, and this can alter secondary fluids and phases [56,57]. Therefore, assuming stochiometric weathering in equilibrium modelling simplifies the complex interplay of geochemical systems by overlooking aspects that may cause shifts in fluid chemistry over time [56]. Therefore, the equilibrium approach only gives insight into the thermodynamic limits and potential reactions, without completely capturing all dynamic processes. Despite these limitations and challenges, the work presented here makes a first important step in simulating the water–rock reactions generating the alkaline fluids of sodium bicarbonate–carbonate in the interior of the Grønnedal-Íka complex.

**Table 4.** Representative water samples from Ikka fjord (b.d. = below detection).

| **Type of Water** | **Sea** | **Stream** | **Spring** | **Column 3** | **Column 2** | **Column 1** | **Modelled Average Column Water** |
|---|---|---|---|---|---|---|---|
| **Area** | **Fjord** | **E-Coast** | **Intrusion** | **Column Fjord** | **Column Fjord** | **Column Fjord** | **Fjord Average** |
| Locality | Snævring | Camp | | Camp | Atoll | Atoll | |
| Temp | 1.3 | 8 | 5 | 3.4 | 3.1 | 4.1 | |
| pH | 7.9 | 7.72 | 8.25 | 10.16 | 10.36 | 10.34 | 10.5 |
| Alkalinity | 2.1 | b.d. | 2.4 | 114 | 179 | 174 | 155 |
| meq/L | $H^+$ | | | | | | |
| $Na^+$ | 437 | 0.15 | 0.11 | 170 | 198 | 252 | 179 |
| $K^+$ | 10.3 | 0.016 | 0.01 | 2.3 | 1.87 | 2.07 | 1.7 |
| $Ca^{2+}$ | 8.83 | 0.055 | 0.988 | 0.09 | 0.17 | 0.24 | 0.2 |
| $Mg^{2+}$ | 45.7 | 0.029 | 0.123 | 2.67 | 1.6 | 2.71 | 0 |
| $Sr^{2+}$ | 0.1 | 0.002 | 0.03 | 0.005 | 0.007 | 0.007 | 0.005 |
| $Cl^-$ | 499 | 0.15 | 0.048 | 59 | 21.2 | 33.8 | 23 |
| $SO_4^{2-}$ | 26.1 | 0.05 | 0.031 | 4.04 | 2.78 | 3.59 | 2.8 |
| $Br^-$ | 0.8 | b.d. | b.d. | 0.41 | 0.43 | 0.42 | 0.38 |
| $PO_4^{3-}$ | b.d. | b.d. | b.d. | 0.093 | 0.26 | 0.24 | 0.17 |
| $SiO_2$ | 0.002 | 0.23 | 0.051 | b.d. | b.d. | b.d. | 0 |
| $NH_4^-$ | | | | | | | |
| $NO_3^-$ | | | | | | | |
| **$SO_4^-$** | | | | | | | |

## 5. Conclusions

Nepheline syenites of the Grønnedal-Íka igneous complex are rich in alkali elements (Na, K) and are classified as calcio-carbonatite, ferruginous carbonatite, or ferro-carbonatite, depending on the FeOt content. The results of the reaction path modelling of dissolving nepheline syenite and either calcio-carbonatite or ferruginous carbonatite at a 1:1 mix are

characterized by the simultaneous precipitation of calcium carbonate minerals (e.g., calcite or ikaite), amorphous manganese oxide, smectite and illite clays, kalsilite, alumina oxide, and goethite, in the case of ferruginous carbonatite. Simple oxides form at the initial stage of the simulation, followed by the precipitation of clays, along with calcite or ikaite, depending on which $CaCO_3$ mineral is chosen for the modelling. The main characteristics of the simulated secondary fluids upon water–rock interaction are highly alkaline waters with pH > 10, a high $Na^+$ concentration, and a low $CO_2$(g) concentration. Major aqueous DIC species of $CO_3^{2-}$, $HCO_3^-$, $NaCO_3$(aq), and other chemical signatures, like pH and the presence of $CaCO_3$(aq) as the main Ca ion species, correlate well with the real fluids sampled from the columns of Ikka Fjord. For the best-fit modelling with real fluid chemistry, it is important to meet the requirement for conditions where atmospheric $CO_2$(g) does not equilibrate with the groundwater. The saturation of the groundwater with ikaite points to a possible alternative method, by which ikaite crystals become seeded in the sediments on the seabed of Ikka Fjord, which could create the nucleation starting points of the column growth.

**Supplementary Materials:** The following supporting information can be downloaded at: https://www.mdpi.com/article/10.3390/min15040373/s1, Table S1: XRF analysis (Wt.%) of major composition of selected carbonatite and nepheline-syenite; Table S2: EMPA analysis for mineral chemistry for representative carbonatites and nepheline syenite; Table S3: EMPA analysis for REE and phosphate mineral chemistry for representative carbonatites and nepheline syenite; Table S4: pH results of batch experiments of syenite, carbonatite and a mixture; Table S5: Results of PhreeqC modelling for secondary waters and phases at 5°C for closed system; Table S6: Results of PhreeqC modelling for secondary waters and phases at 5°C for open system.

**Author Contributions:** Conceptualization, S.M.A., G.J.S., E.S., E.B. and A.S.; methodology, S.M.A., E.B., G.H.G. and A.S.; software, S.M.A. and G.H.G.; validation, E.B. and G.H.G.; formal analysis, S.M.A. and G.H.G.; investigation, S.M.A.; resources, G.J.S., E.B. and A.S.; data curation, S.M.A. and G.H.G.; writing—original draft preparation, S.M.A. and G.J.S.; writing—review and editing, S.M.A., G.J.S., E.S., E.B., G.H.G. and A.S.; visualization, S.M.A. and E.S.; supervision, G.J.S., E.S., E.B. and A.S.; project administration, G.J.S., E.B. and A.S.; funding acquisition, G.J.S. All authors have read and agreed to the published version of the manuscript.

**Funding:** This research was funded by Aase og Jørgen Münters Fond, grant 2019, Aage V. Jensens Fond, grant 2019, Eggertsjóður, grant 2018, the University of Iceland's Research Fund, grants 2019 and 2020, and Carl Tryggers Stiftelse, grant number CTS 20:1579.

**Data Availability Statement:** The raw data supporting the conclusions of this article will be made available by the authors on request.

**Acknowledgments:** We would like to acknowledge and thank Eggertsjóður and the University of Iceland's Research Fund in Iceland, the Bolin Centre for Climate Research and Carl Tryggers Stiftelse in Sweden, and Aase og Jørgen Münters Fond and Aage V. Jensens Fond in Denmark for their financial support to the Ikka project in 2018–2019. Furthermore, we would like to thank the Joint Arctic Command (JACO), Station Grønnedal, and the crew of F360 HVIDBJØRNEN for their excellent logistical and diving support in 2019, as well as our IKKA colleagues Paul Seaman and Richard Gyllencreutz for their valuable scientific contributions to the 2019 fieldwork. Our sincere thanks go to Nicholas Odling at the University of Edinburgh for carrying out the whole rock analysis and to technicians Sveinbjörn Steinþórsson, Rebekka Hlín Rúnarsdóttir, and Jóhann Gunnarsson Robin at the University of Iceland for assisting in the thin section preparation and powder preparation for the whole rock analysis. This work was carried out under scientific survey license Nos. VU-00154 and VU-00127 and export permit No. 180/2018, issued by the Mineral License and Safety Authority (MLSA) in Greenland. Finally, we would like to thank the three anonymous reviewers for their constructive comments, which helped improve the quality of this paper.

**Conflicts of Interest:** The authors declare no conflicts of interest.

## References


1. Buchardt, B.; Seaman, P.; Stockmann, G.; Vous, M.; Wilken, U.; Düwel, L.; Kristiansen, A.; Jenner, C.; Whiticar, M.J.; Kristensen, R.M. Submarine columns of ikaite tufa. *Nature* **1997**, *390*, 129–130.
2. Buchardt, B.; Israelson, C.; Seaman, P.; Stockmann, G. Ikaite tufa towers in Ikka Fjord, Southwest Greenland: Their formation by mixing of seawater and alkaline spring water. *J. Sediment. Res.* **2001**, *71*, 176–189.
3. Seaman, P.; Buchardt, B. The columns of ikate tufa in Ikka Fjord, Greenland. *Geosci. Monogr. Greenl.* **2006**, *44*, 39.
4. Hansen, M.O.; Buchardt, B.; Kühl, M.; Elberling, B. The fate of Submarine Ikaite Tufa Columns in Southwest Greenland Under Changing Climate Conditions. *J. Sediment. Res.* **2011**, *81*, 553–561. [CrossRef]
5. Stockmann, G.J.; Seaman, P.; Balic-Zunic, T.; Peternell, M.; Sturkell, E.; Liljebladh, B.; Gyllencreutz, R. Mineral Changes to the Tufa Columns of Ikka Fjord, SW Greenland. *Minerals* **2022**, *12*, 1430. [CrossRef]
6. Tollefsen, E.; Stockmann, G.; Skelton, A.; Lundqvist, L.; Sturkell, E. Secondary alteration of the Gronnedal-Ika igneous complex and the genesis of ikaite, $CaCO_3$ $6H_2O$, SW Greenland. *Chem. Geol.* **2019**, *510*, 18–30.
7. Söderlund, U.; Isachsen, C.E.; Bylund, G.; Heaman, L.M.; Jonathan Patchett, P.; Vervoort, J.D.; Andersson, U.B. U–Pb baddeleyite ages and Hf, Nd isotope chemistry constraining repeated mafic magmatism in the Fennoscandian Shield from 1.6 to 0.9 Ga. *Contrib. Mineral. Petrol.* **2005**, *150*, 174–194.
8. Ernst, R.E.; Wingate, M.T.; Buchan, K.L.; Li, Z.X. Global record of 1600-700 Ma Large Igneous Provinces (LIPs): Implications for the reconstruction of the proposed Nuna (Columbia) and Rodinia supercontinents. *Precambrian Res.* **2008**, *160*, 159–178.
9. Siegel, K.; Williams-Jones, A.E.; Stevenson, R. A Nd- and O-isotope study of the REE-rich peralkaline Strange Lake granite: Implications for Mesoproterozoic A-type magmatism in the Core Zone (NE-Canada). *Contrib. Mineral. Petrol.* **2017**, *172*, 54. [CrossRef]
10. Pandey, R.; Rao, N.V.C.; Dhote, P.; Pandit, D.; Choudhary, A.K.; Sahoo, S.; Lehmann, B. Rift associated ultramafic lamprophyre (damtjernite) from the middle part of the Lower Cretaceous (125 Ma) succession of Kutch, northwestern India: Tectonomagmatic implications. *Geosci. Front.* **2017**, *9*, 1883–1902. [CrossRef]
11. Pandey, R.; Rao, N.V.C.; Singh, M.K.; Talukdar, D. Alkaline rocks from the Deccan Large Igneous Province: Time–space distribution, petrology, geochemistry and economic aspects. *J. Earth Syst. Sci.* **2022**, *131*, 108. [CrossRef]
12. Stockmann, G.; Karlsson, A.; Lewerentz, A.; Thomsen, T.B.; Kokfelt, T.F.; Tollefsen, E.; Sturkell, E.; Lundqvist, L. New Rb–Sr and zircon U–Pb dating of the Grønnedal-Íka igneous complex, SW Greenland. In Proceedings of the Nordic Geological Winter Meeting 2018, Copenhagen, Denmark, 10–12 January 2018; p. 38.
13. Beard, C.D.; Finch, A.A.; Borst, A.M.; Goodenough, K.M.; Hutchison, W.; Millar, I.L.; Andersen, T.; Williams, H.M.; Weller, O.M. A phlogopite-bearing lithospheric mantle source for Europe's largest REE-HFSE belt: Gardar Rift, SW Greenland. *Earth Planet. Sci. Lett.* **2024**, *60*, 11.
14. Upton, B.G.J.; Emeleus, C.H.; Heaman, L.M.; Goodenough, K.M.; Finch, A.A. Magmatism of the mid-Proterozoic Gardar Province, South Greenland: Chronology, petrogenesis and geological setting. *Lithos* **2003**, *68*, 43–65. [CrossRef]
15. Hanzelmann, L. REE Mobility During Late-Stage Hydrothermal Alteration in the Siderite Carbonatites of the 1.3 Ga Grønnedal-Íka Alkaline Complex, Southwest Greenland. Master's Thesis, Institute of Applied Mineralogy and Economic Geology, RWTH Aachen University, Aachen, Germany, 2022; 159p.
16. Garde, A.A.; Hamilton, M.A.; Chadwick, B.; Grocott, J.; McCaffrey, K.J.W. The Ketilidian orogen of South Greenland: Geochronology, tectonics, magmatism, and fore-arc accretion during Palaeoproterozoic oblique convergence. *Can. J. Earth. Sci.* **2002**, *39*, 765–793. [CrossRef]
17. Garde, A.A.; Chadwick, B.; Grocott, J.; Hamilton, M.A.; McCaffrey, K.J.W.; Swager, C.P. Mid-crustal partitioning and attachment during oblique convergence in an arc system, Palaeoproterozoic Ketilidian orogen, southern Greenland. *J. Geol. Soc.* **2002**, *159*, 247–261. [CrossRef]
18. Escher, A.; Watt, W.S. (Eds.) Summary of the geology of Greenland. In *Geology of Greenland*; Grønlands Geologiske Undersøgelse: Copenhagen, Denmark, 1976; pp. 10–16.
19. Emeleus, C.H.; Upton, B.G.J. The Gardar period in South Greenland. In *Geology of Greenland*; Escher, A., Watt, W.S., Eds.; Grønlands Geologiske Undersøgelse: Copenhagen, Denmark, 1976; pp. 152–181.
20. Upton, B.G.J. Tectono-magmatic evolution of the younger Gardar southern rift, South Greenland. *Geol. Surv. Den. Greenl. Bull.* **2013**, *29*, 4692. [CrossRef]
21. Emeleus, C.H. The Gronnedal-Ika alkaline complex, South Greenland. The structure and geological history of the complex. *Bull. Grønl. Geol. Unders.* **1964**, *45*, 78. [CrossRef]
22. Bartels, A.; Nilsson, M.K.M.; Klausen, M.B.; Söderlund, U. Meso-proterozoic dykes in the Timmiarmiit area, Southeast Greenland: Evidence for a continuous Gardar dyke swarm across Greenland's North Atlantic Craton. *GFF* **2016**, *138*, 255–275. [CrossRef]

23. Ranta, E.; Stockmann, G.; Wagner, T.; Fusswinkel, T.; Sturkell, E.; Tollefsen, E.; Skelton, A. Fluid-Rock reactions in the 1.3 Ga siderite carbonatite of the Grønnedal-Íka alkaline complex, Southwest Greenland. *Contrib. Mineral. Petrol.* **2018**, *173*, 1–28. [CrossRef]
24. Bedford, C.M. The Mineralogy, Geochemistry, and Petrogenesis of the Gronnedal-íka Alkaline Igneous Complex, South-West Greenland. Ph.D. Thesis, Durham University, Durham, UK, 1990.
25. Woolley, A.R.; Kjærsgaard, B.A. Paragenetic types of carbonatite as indicated by the diversity and relative abundances of associated silicate rocks: Evidence from a global database. *Can. Mineral.* **2008**, *46*, 741–752. [CrossRef]
26. Seaman, P.; Sturkell, E.; Gyllencreutz, R.; Stockmann, G.J.; Geirsson, H. New multibeam mapping of the unique *Ikaite* columns in Ikka Fjord, SW Greenland. *Mar. Geol.* **2022**, *222*, 106710. [CrossRef]
27. Buchardt, B.; Stockmann, G.; Hansen, M.O.; Sveinbjörnsdóttir, Á. Isotope hydrology ($^{2}H$ and $^{18}O$) of Ikka fjord and its tufa columns, SW Greenland. *Geol. Soc. Den.* **2024**, *73*, 22.
28. Ohmura, A.; Reeh, N. New precipitation and accumulation maps for Greenland. *J. Glaciol.* **1991**, *37*, 140–148.
29. Buch, E. Havstrømme omkring Grønland. In *Grønlands Fysiske Natur*; Gregersen, S., Ed.; København: Rhodos, Denmark, 1995; pp. 25–32.
30. Bischoff, J.L.; Fitzpatrick, J.A.; Rosenbauer, R.J. The solubility and stabilization of ikaite ($CaCO_3 \cdot 6H_2O$) from 0 °C to 25 °C: Environmental and paleoclimatic implications for thinolite tufa. *J. Geol.* **1993**, *101*, 21–33.
31. Stockmann, G.; Tollefsen, E.; Skelton, A.; Brüchert, V.; Balic-Zunic, T.; Langhof, J.; Skogby, H.; Karlsson, A. Control of calcite inhibitor (phosphate) and temperature on ikaite precipitation in Ikka fjord, southwest Greenland. *Appl. Geochem.* **2018**, *89*, 11–22.
32. Tollefsen, E.; Stockmann, G.; Skelton, A.; Mörth, C.-M.; Dupraz, C.; Sturkell, E. Chemical controls on ikaite formation. *Mineral. Mag.* **2018**, *82*, 1119–1129. [CrossRef]
33. Trampe, E.C.; Richard, W.; Castenholz, J.; Larsen, E.; Michael Kuhl, M. Phototrophic microbes form endolithic biofilms in ikaite tufa columns (SW Greenland). *Environ. Microbiol.* **2017**, *19*, 4754–4770.
34. Marland, G. The stability of $CaCO_3 \cdot 6H_2O$ (ikaite). *Geochim. Cosmochim. Acta* **1975**, *39*, 83–91.
35. Dahl, K.; Buchardt, B. Monohydrocalcite in the Arctic Ikka fjord, SW Greenland: First reported marine occurrence. *J. Sed. Res.* **2006**, *76*, 460–471.
36. Garvie, L. Seasonal formation of ikaite in slime flux jelly on an infected tree (*Populus fremontii*) wound from the Sonoran Desert. *Sci. Nat.* **2022**, *109*, 48. [CrossRef]
37. Vickers, M.L.; Vickers, M.; Rickaby, R.E.; Wu, H.; Bernasconi, S.M.; Ullmann, C.V.; Bohrmann, G.; Spielhagen, R.F.; Kassens, H.; Schultz, B.P.; et al. The ikaite to calcite transformation: Implications for palaeoclimate studies. *Geochim. Cosmochim. Acta* **2022**, *334*, 201–216.
38. Rantanen, M.; Karpechko, A.Y.; Lipponen, A.; Nordling, K.; Hyvärinen, O.; Ruosteenoja, K.; Vihma, T.; Laaksonen, A. The Arctic has warmed nearly four times faster than the globe since 1979. *Commun. Earth Environ.* **2022**, *3*, 168.
39. Jarosewich, E. Smithsonian microbeam standards. *J. Res. Natl. Inst. Stand. Technol.* **2002**, *107*, 681.
40. Armstrong, J.T. *Electron Probe Quantitation*; Heinrich, K.F.J., Newbury, D.E., Eds.; Plenum Press: New York, NY, USA, 1991; p. 261.
41. Parkhurst, D.L.; Appelo, C.A.J. *User's Guide to PHREEQC (Version 2)—A Computer Program for Speciation, Batch-Reaction, One-Dimensional Transport, and Inverse Geochemical Calculations*; Report 99-4259; Water- Resources Investigations; U.S. Geological Survey: Reston, VA, USA, 1999.
42. Voigt, M.; Marieni, C.; Clark, D.E.; Gíslason, S.R.; Oelkers, E.H. Evaluation and refinement of thermodynamic databases for mineral carbonation. *Energy Procedia* **2018**, *146*, 81–91. [CrossRef]
43. Parkhurst, D.L.; Appelo, C.A.J. Description of input and examples for PHREEQC version 3—A computer program for speciation, batch-reaction, one-dimensional transport, and inverse geochemical calculations. *US Geol. Surv. Tech. Methods* **2013**, *6*, 497.
44. Krupka, K.M.; Cantrell, K.J.; McGrail, B.P. *Thermodynamic Data for Geochemical Modeling of Carbonate Reactions Associated with CO2 Sequestration—Literature Review*; Prepared for the U.S. Department of Energy; (PNNL-19766); Pacific Northwest National Laboratory Richland: Washington, DC, USA, 2010.
45. Keiding, K.; Heidam, N.Z. Observations on acidity and ions in East Greenland precipitation, Tellus, B. *Chem. Phys. Meteorol.* **1986**, *38*, 345–352. [CrossRef]
46. Middlemost, E.A.K. Naming materials in the magma/igneous rocks system. *Earth Sci. Rev.* **1994**, *37*, 215–224. [CrossRef]
47. Gittins, J.; Harmer, R.E. What is ferrocarbonatite? A revised classification. *J. Afr. Earth Sci.* **1997**, *25*, 159–168.
48. Heinrich, E.W. *The Geology of Carbonatites*; Rand McNally & Co.: Chicago, IL, USA, 1966.
49. Gill, R.C.O. The Geochemistry of the Gronnedal-ika Alkaline Complex, South Greenland. Ph.D. Thesis, Durham University, Durham, UK, 1972.
50. Tole, M.P.; Lasaga, A.C.; Pantano, C.; White, W.B. The kinetics of dissolution of nepheline ($NaAlSiO_4$). *Geochim. Cosmochim. Acta* **1986**, *50*, 379–392.
51. Stockmann, G.J.; Ranta, E.; Trampe, E.; Sturkell, E.; Seaman, P. Carbon mineral storage in seawater: Ikaite ($CaCO_3$ $6H_2O$) columns in Greenland. *Energy Procedia* **2018**, *146*, 59–67.

52. Seymour, L.M.; Maragh, J.; Sabatini, P.; Di Tommaso, M.; Weaver, J.C.; Masic, A. Hot mixing: Mechanistic insights into the durability of ancient Roman concrete. *Sci. Adv.* **2023**, *9*, eadd1602. [CrossRef] [PubMed]
53. Mackenzie, F.T.; Lerman, A. *Carbon in the Geobiosphere: Earth's Outer Shell*; Springer: Dordrecht, the Netherlands, 2006; p. 402.
54. Seaman, P.G. The Development of Ikaite in a Fjord Environment with Special Reference to Ikka Fjord. Unpublished. Ph.D. Thesis, Imperial College of Science, Technology and Medicine, University of London, London, UK, 1998; p. 263.
55. Lasaga, A.C. *Kinetic Theory in Earth Sciences*; Princeton University Press: Princeton, NJ, USA, 1998.
56. Drever, J.I. *The Geochemistry of Natural Waters: Surface and Groundwater Environments*; Prentice Hall: Hoboken, NJ, USA, 1997.
57. White, A.F. Chemical Weathering Rates of Silicate Minerals in Soil. In *Chemical Weathering Rates of Silicate Mineral*; White, A.F., Brantley, S.L., Eds.; Mineralogical Society America, Reviews in Mineralogy: Washington, DC, USA, 1995; Volume 31, pp. 407–461. [CrossRef]

**Disclaimer/Publisher's Note:** The statements, opinions and data contained in all publications are solely those of the individual author(s) and contributor(s) and not of MDPI and/or the editor(s). MDPI and/or the editor(s) disclaim responsibility for any injury to people or property resulting from any ideas, methods, instructions or products referred to in the content.